Gelatin-Nanodiamond Hydrogel for Drug Delivery and Bone Tissue Engineering

By

Ryan Maloney

Submitted to the graduate degree program in Bioengineering and the Graduate Faculty of the University of Kansas School of Engineering in partial fulfillment of the requirements for the degree of Master of Science.

_____

Dr. Arghya Paul, Committee Chair

_____

Dr. Michael Detamore

_____

Dr. Cory Berkland

_____

Dr. Stevin Gehrke

Date Defended: June 7, 2016

The Thesis Committee for Ryan Maloney

Certifies that this is the approved version of the following thesis:

Gelatin-Nanodiamond Hydrogel for Drug Delivery and Bone Tissue Engineering

_____

Dr. Arghya Paul, Committee Chair

Date approved: June 7, 2016

Abstract

As one of the few human tissues to recover without scars, bone's capacity to remodel itself and recover from injury is undoubtedly impressive. However, non-union fractures and critical sized defects, often the result of trauma, disease-related fractures, and tumor resection, have great difficulty healing without intervention. Common treatments for these maladies include using bone autografts and allografts to fill the defect, though each of these treatments have their own potential complications and drawbacks. Tissue engineering strategies aim to recreate bone or bone's natural healing processes on a lab-made scaffold along with cells and therapeutics for implantation. In addition, recreation of bone-like functions by improving *in vitro* models is crucial for drug testing and mechanistic studies. One class of materials used for both therapeutics and *in vitro* modeling are hydrogels, water-swollen polymeric networks that often exhibit great biocompatibility due to their similarity to native extracellular matrix. Hydrogels' fragile mechanical properties relative to the remarkable strength of bone limit their application in heavy load-bearing regions of bone. Including nanomaterials within the polymeric network can both increase the strength of the network and allow exploitation of their unique abilities to interact with encapsulated cells and therapeutics. Here, we hypothesize that the inclusion of nanodiamonds, octahedral carbon-based nanoparticles, can both improve the mechanical properties of a gelatin methacrylamide system and enable dexamethasone loading and delivery to encapsulated human adipose-derived mesenchymal stem cells. In the first section, we review bone tissue engineering strategies with a focus on hydrogels and carbon nanomaterials. In the second section, this project and its results are reported and analyzed, and finally, ideas for future work with nanodiamonds and hydrogels are discussed.

Table of Contents

Chapter 1

Introduction: A Review of Bone Tissue Engineering

1.1 Abstract

Bone's natural healing capacity is seriously hampered and often nonexistent in the case of nonunion fractures and critical-sized defects. Often the result of serious trauma or tumor resection, both critical-sized defects and nonunion fractures are unable to heal without intervention. Autografts and allografts are the current major treatment options to aid in bone recovery, but both carry drawbacks and can result in serious complications. Bone tissue engineering strategies aim to eliminate these by using rationally designed scaffolds that enhance healthy bone regrowth into defects. Combining scaffolds with therapeutics, be they drugs, proteins, or cells, enriches the healing capacity of the scaffold and is the subject of intense research. One class of promising scaffolding material are hydrogels, composed of a hydrophilic polymeric network that closely resembles extracellular matrix, have high biocompatibility, tunable physical and mechanical properties, and the ability to encapsulate therapeutics and cells within the network. However, unmodified hydrogels frequently have low compressive elastic moduli as well as fracture strength that limit their efficacy in load-bearing defects. Including nanomaterials within hydrogels can enhance their mechanical properties due to interaction between material and polymer and can also modulate therapeutic loading and release. Carbon nanomaterials, such as graphene, carbon nanotubes, and nanodiamonds, have attracted broad attention in tissue engineering due to their unique properties. Integrating carbon nanomaterials and hydrogels allows researchers to take advantage of these properties. Here, we discuss bone physiology, general bone tissue engineering strategies, hydrogels for bone tissue engineering, and finally the potential use of carbon nanomaterials in bone tissue engineering.

1.2 Bone Physiology and Disease

Healthy bone orchestrates an impressive variety of physiological tasks. Its most obvious role is protecting internal organs and providing support for movement thanks to its superb compressive and tensile strength, with a Young's modulus ranging from 12-25 GPa [1] in cortical bone and 0.1-0.5 GPa [2] in cancellous bone. Bone and bone marrow also produce blood and aid in its pH regulation, act as a store for minerals, and host mesenchymal and hematopoietic stem cells. Composed of ~40% type I collagen fibers and ~50% hydroxyapatite crystals, bone's anisotropic composite structure results in great compressive strength. Collagen fibers, parallel to the direction of compressive stress, are decorated in an ordered fashion with plate-like hydroxyapatite crystals with dimensions of around 2x30x40 nm [3, 4]. Both cortical and cancellous bone play vital roles in bone physiology. Cortical bone, which forms the outer shell of bones, is significantly denser than its counterpart and thus is crucial to load bearing and movement. Cancellous bone is located at the ends of long bones such as the femur and performs bone's other functions. These other tasks are just as crucial as load bearing; cancellous bone is highly vascularized to support calcium exchange with the blood and is awash with red bone marrow containing hematopoietic and mesenchymal stem cells. At the cellular level, osteoblasts, osteoclasts, and osteocytes contribute to bone homeostasis by overseeing a fine balance of type I collagen and hydroxyapatite deposition and remodeling. A disruption of this balance by a wide variety of factors can lead to diseases such as osteoporosis and osteoarthritis.

When bone is damaged by a fracture or medical procedure, it is normally able to heal itself effectively by intramembranous and endochondral ossification. Initially, a hematoma forms around the fracture and infiltrating macrophages and osteoclasts remove damaged pieces of bone and other tissue. In intramembranous ossification, the periosteum, the fibrous, outermost layer of bone, releases progenitor cells to form a bony callous around the periphery of each side of the

fracture, while the process of endochondral ossification bridges the gap between fracture ends by forming a fibrous cartilaginous matrix. After these processes are complete, blood vessels infiltrate the callus and the cartilaginous matrix is resorbed as new bone is deposited in its place to form a hard callus throughout the fracture and around its periphery. Finally, normal homeostatic osteoblast and osteoclast turnover resorbs excess bone from the callus and deposits new matrix in its place; this property of bone is unique among human tissue, as no scar formation occurs after fracture [5, 6].

Though bone has an impressive capacity to heal naturally, an array of diseases present physicians and surgeons with numerous hurdles for effective treatment. Major degenerative diseases such as osteoporosis and osteoarthritis and their increased risk of serious fractures [7, 8] plague our quickly growing elderly population; total joint replacements have increased dramatically over the last 15 years [9, 10]. Demand continues to grow, with total amounts of both knee and hip arthroplasty procedures growing by ~6% from 2009-10 [11]. Less prevalent diseases such as congenital osteogenesis imperfecta and temporary or chronic bacterial infections in osteomyelitis also present a serious burden on patients. Orthopedic surgeons are faced with the effects of not just osteoarthritis, osteoporosis, and other common bone diseases, but must address difficult-to-treat traumatic bone fractures. In addition, resection of primary and secondary bone tumors by surgeons often requires removal of significant portions of bone tissue [12].

In many cases after surgery, bone is unable to heal normally. Difficulty healing due to infection or poor blood supply after a total joint replacement can result in a nonunion fracture, in which a fracture does not rejoin despite mechanical fixation. Nonunion fractures typically require surgical intervention for treatment [13]. Critical-sized defects are commonly caused by trauma and resection of tumors; this term is used to describe a void of tissue that will not heal

without treatment [14]. The current standard treatments for critical sized defect, bone autografts and allografts, have numerous drawbacks. In the case of autografts, tissue must first be removed from a secondary site, usually the pelvis, and used to fill the defect. Complications from autografts can include morbidity, pain, and infection at both the secondary site and the defect site; in addition, a lack of available healthy donor tissue can restrict the supply of autograft [15, 16]. Allografts eliminate the need for a donor site and have reduced issues with supply, but carry their own drawbacks as well: donor tissue can risk disease transmission [17], infect the patient [18], or induce a patient inflammatory response to the implanted tissue. In addition, allografts typically do not integrate with host tissue as successfully as autografts do [19]. Greater than 2 million bone grafts are performed every year worldwide [20], each with these potential risks. For these reasons, tissue engineering researchers have sought to create significantly better alternatives to grafting for the repair of critical-sized defects and to aid in the healing process for non-union fractures. In addition to their goals to eventually replace tissue and current grafting technology, tissue engineers also aim to develop better *in vitro* models of bone and bone diseases for mechanistic studies and drug discovery and testing. In the following sections, we overview current strategies in this field, with a focus on biopolymers, and finally hydrogels and nanocomposite hydrogels for therapeutic use and modeling.

1.3 Bone Tissue Engineering Strategies

Using biomimetic synthetic scaffolds, to replace critical-sized defects and aid in the repair of non-unions has the potential to solve the issues presented by autograft and allograft use. Using synthetic or abundant biologically-derived materials like gelatin, of which researchers possess unlimited amounts compared to typical grafting materials, eliminates the issues to which both autografts and allografts are prone. In their review of biomimetic bone tissue engineering,

Porter *et al*. listed a daunting eleven requirements for a perfect tissue engineered bone replacement [21]. To summarize, it must provide mechanical support while the tissue heals and encourage self-integration with surrounding tissue, be porous enough for vascularization and cellular infiltration, promote osteogenic differentiation of infiltrating mesenchymal stem cells, have a controlled degradation profile without releasing toxic or inflammatory products, and finally deliver therapeutics or cells in a controlled, effective fashion. Several major scaffold types, porous and fibrous scaffolds along with hydrogels, composed of wide-ranging synthetic polymers [22] and biopolymers [23] have been the focus of research in this field. Polymers are frequently combined with ceramics, bioactive glasses, and nanomaterials in attempts to recreate the composite structure of bone [24, 25]. Combining these scaffolds with cells, therapeutics, or both can enhance their regenerative capabilities significantly [21]. Mesenchymal stem cells (MSCs) normally migrate to damaged bone, and when included in a scaffold can both modulate the host response to an implant *in vivo* and differentiate along chondrogenic or osteogenic lineages to speed healing [26, 27]. Drugs such as the osteoinductive dexamethasone [28], proteins of the bone morphogenetic protein family and vascularization enhancers like platelet-derived growth factor [29], and nucleic acids as plasmids or siRNA [30, 31] are a few examples of therapeutics used in concert with scaffolds and cells. The available strategies for bone tissue engineering are presented in Figure 1.1. In the following sections, we offer a brief review and several examples of the major components of the project presented in Chapter 2. A variety of biopolymers, including the gelatin used in this project, for bone tissue engineering are presented in the next section. Next, we present several examples and the advantages and disadvantages of using biopolymer hydrogels in bone tissue engineering. Finally, a brief overview of filling agents

leads us into a discussion of carbon nanomaterials, in particular nanodiamonds, and the presentation of our work in the following chapter.

1.3.1 Biopolymers for Bone Tissue Engineering

Biopolymers, including structural proteins, glycosaminoglycans (GAGs), or polysaccharides, frequently exhibit superior biocompatibility to synthetic polymers. Infiltration, adhesion, and migration of cells within biopolymer scaffolds is significantly easier. However, concerns remain about their reduced versatility compared to synthetic polymers, batch to batch variability, and potential immunogenicity of non-human biopolymers remain. Though biopolymers inherently have less versatility than synthetic ones, creative chemical modifications and scaffold fabrication strategies by researchers have resulted in impressive flexibility. For example, solvent casting, particulate leaching, and 3D printing have been used to create and modify porous scaffolds and hydrogels [32], while electrospinning can create a wide variety of polymeric nanofibers [33]. Several of the most attractive and widely used biopolymers are alginate, chitosan, hyaluronic acid, and collagen/gelatin. Alginate, an anionic polysaccharide derived from brown algae, displays excellent biocompatibility and quick and simple gelation. Alginate microspheres crosslinked with calcium chloride have shown encouraging applications: Zhao *et al*. combined calcium phosphate paste with alginate-based microspheres encapsulating umbilical cord mesenchymal stem cells (hUCMSCs); this system showed both mechanical properties on the order of cancellous bone and effective differentiation of the hUCMSCs into osteoblasts [34]. Chitin is a structural, cationic polysaccharide that can be extracted from insects and crustaceans, then hydrolyzed to chtosan. Collagen/chitosan thermogels have been created by using β-glycerophosphate, normally used as an osteogenic supplement, as an ionic crosslinking agent [35]. As a GAG, hyaluronic acid is usually used in cartilage tissue engineering [36];

studies attempting osteochondral interface development frequently utilize it. Patterson *et al*. studied glicidyl-methacrylate modified hyaluronic acid hydrogels codelivering BMP-2 and vascular endothelial growth factor (VEGF) with different degradation rates, finding that the most quickly and most slowly degrading hydrogels showed increased new bone formation [37]. Collagen and gelatin, as derivatives of the major structural protein of bone, are perhaps the most attractive options for future clinical translation. Collagen is composed of three α-helices of the form Gly-X-Y with very frequent proline and hydroxyproline residues. These helices themselves self-assemble into triple helices, which further assemble into collagen fibrils that are enzymatically crosslinked *in vivo*. Gelatin is simply denatured collagen, whereby heat and an acid or base treatment has been used to hydrolyze crosslinks, resulting in a randomly coiled structure. Both polymers, as one might expect, show high biocompatibility with many cell lines, given the multitude of cellular adhesion sites for cell traction and migration. In the chitosan/collagen composite study previously mentioned, the inclusion of collagen allowed for significantly enhanced cell proliferation. Cellular DNA content in pure chitosan scaffolds halved over the course of two weeks, while the addition of collagen helped double the amount of DNA in the scaffold over the same time [35]. Combining collagen/gelatin and various hydroxyapatite materials has been a successful strategy. Perez *et al.* crafted gelatin/hydroxyapatite microspheres using a water-in-oil immersion method [38] that could be used for controlled delivery of osteogenic factors. Gelatin inclusion enabled excellent cellular adhesion and proliferation compared to hydroxyapatite spheres alone. Though recombinant BMP-2 (rBMP-2) is an FDA-approved treatment in spinal fusion products, its uncontrolled release into surrounding tissues has led to serious side effects. Collagen, nanohydroxyapatite (nHA), and alginate microspheres containing rBMP-2 were used to create a porous scaffold interspersed with microspheres.

Alginate microspheres resulted in significantly greater extension and control over growth factor release [39]. Biopolymers can be used to create a variety of scaffold types, including remarkably versatile hydrogels. In the next section, we overview hydrogels and their applications and limits in bone tissue engineering.

1.3.2 Hydrogels for Bone Tissue Engineering

Hydrogels are composed of a water-swollen network of typically randomly arranged hydrophilic polymer chains that more closely recapitulates native ECM than the fibrous or porous scaffolds mentioned above. From both synthetic polymers and biopolymers, tissue engineers have created hydrogels with tunable mechanical properties [40], porosities [32], and degradation profiles [37, 41] to mimic targeted tissues and control therapeutic delivery. In addition, numerous physical and chemical crosslinking methods allow control over gelation conditions. In particular, photocrosslinkable and thermogelling hydrogels are promising for eventual application in regenerative medicine; the ease of cell encapsulation along with the injectability of their prepolymer solution easily delivers cells to the target site and allows for filling of iregullar defects [35, 42]. Hydrogels are also a valuable tool for creating more sophisticated 3D cell culture techniques in efforts to enhance the accuracy and thus add applicability to *in vitro* studies [43, 44]. With applications such as the generation of microvascular networks [45], microgel fabrication to study differentiation processes [46], and regenerative medicine approaches for numerous tissues [42], gelatin methacrylamide (GelMA), used in this study, is one example of a photocrosslinkable polymer with applications in both therapeutics and novel *in vitro* constructs.

Unfortunately, hydrogels generally lack both the compressive strength and fracture properties of more robust fibrous and porous scaffolds, and this can limit their application in

heavy load-bearing defects. As a result, hydrogels have been explored as an option for filling in craniofacial defects from trauma or tumor resection, in which their reduced mechanical properties are not a significant liability [47, 48]. In addition, several recent studies suggest that exploiting the natural healing process by implanting a scaffold that stimulates endochondral ossification and encourages vascularization may be a more effective strategy for treatment than implanting simply bone-like scaffolds [49-52]. Hydrogels, with their controllable porosity and degradation profiles, have the properties needed to facilitate vascularization and emulate endochondral ossification. Hyaluronic acid hydrogels and GelMA hydrogels containing MSCs primed for chondrogenesis by inclusion of decellularized cartilage particles have been used for this purpose [50, 51]. One particularly interesting approach was a spheroid coculture of human umbilical vein endothelial cells (HUVECs) and MSCs stimulated by Sonic Hedgehog (Shh) combined within a calcium phosphate and collagen hydrogel. Shh is a crucial morphogen during embryonic development, but also vital for neovascularization [53]. Rivron *et al.* hypothesized that enhanced vascularization would direct a defect to begin endochondral ossification and then mature into bone, and proved this *in vivo* [54].

Despite their emerging potential with regards to endochondral ossification, it is still vital to improve hydrogel mechanical properties to realize further application to bone and other tissues. For this reason, exploiting filling agents, especially nanomaterials, is an attractive option for enhancing their mechanical properties while taking advantage of the diverse chemical and biological capabilities nanomaterials can offer. As they are with other scaffold types, hydroxyapatite and clay materials are excellent filling agents for hydrogel-based bone applications. PEG diacrylate (PEGDA) and GelMA have both been used in combination with discoidal silicate nanoparticles (Laponite). The Laponite both enhanced the mechanical

properties of the GelMA and PEGDA and promoted osteogenic differentiation of encapsulated preosteoblasts in the GelMA system [55, 56]. Fu *et al.* combined collagen and nHA with an injectable, thermogelling copolymer (PEG-PCL-PEG), and implantation in rabbits showed favorable, nearly complete regeneration of a critical-sized defect [57]. These materials are excellent for strategies to emulate the biphasic organic/inorganic nature of bone, but other tools such as carbon nanomaterials offer very unique properties and functionalization strategies for therapeutic delivery and can enhance the mechanical properties of scaffolds.

1.3.3 Carbon Nanomaterials for Bone Tissue Engineering

Carbon nanomaterials, including graphene and graphene oxide (GO), single- and multi-walled carbon nanotubes (CNTs), and nanodiamonds (NDs), are another class of nanomaterials which have been explored for bone tissue engineering and drug delivery purposes. These materials offer several advantages over the typically used calcium phosphate minerals, biogalsses, and nanoscale clay. Firstly, the unique mechanical, electrical, and optical properties of the carbon nanomaterials offer unique opportunities across all tissue engineering disciplines. In addition, they have much more versatile functionalization strategies and therefore the potential to deliver many therapeutic classes in a variety of ways. Graphene has been shown to aid in neuronal, cardiomyogenic, and osteogenic differentiation of related progenitor cells [58-60]. GO, when grafted onto titanium implants, was able to adsorb significant amounts of BMP-2 and differentiate MSCs resulting in enhanced bone repair *in vivo* [61]. Multi-walled CNTs have also been shown to induce osteogenic differentiation of mesenchymal stem cells [62]. Carboxylated MWCNTs modified the physical properties of chitosan/hydroxyapatite scaffolds by electrostatic interactions with chitosan, increasing the thermal stability, porosity, and improving the growth rates of cultured osteoblasts [63].

Though CNTs and graphene have been used in bone tissue engineering, exploration of NDs for use in tissue engineering scaffolds has been limited. NDs are carbon nanoparticles, typically around ~5 nm but with some larger varieties, with a core of diamond lattice and a variety of surface moieties [64]. Traditionally derived from detonation of explosive mixtures with a negative oxygen balance, NDs have been synthesized in a variety of ways in recent years [64]. Perhaps the most attractive aspect of NDs is their versatile surface chemistry. Carboxylated, hydroxylated, hydrogenated, and amine-functionalized NDs are just a few of the many possible surface modifications [65]. In addition, NDs are significantly less toxic than other carbon nanomaterials [66]. To date, biomedical research using NDs has focused mostly on systemic administration of NDs with surface-functionalized drugs as well as fluorescent NDs for applications in cancer therapy and diagnostics. ND/doxorubicin complexes reduced tumor size in a mouse model more effectively than doxorubicin alone, likely due to tropism towards tumors by the enhanced permeability and retention effect and avoidance of drug efflux pumps once inside the cell [67]. NDs with highly carboxylated surfaces have been used to deliver plasmid DNA [31] and siRNA [68]. Initial complexation with positively charged polyethyleneimine (PEI) allows the NDs to then associate with negatively charged nucleic acid chains. Several groups have also reported protein complexation with NDs. Figure 1.2 visualizes these different drug delivery strategies. Moore *et al.* complexed both basic fibroblast growth factor (bFGF) and BMP2 to NDs simultaneously; the complex initiated osteogenic differentiation and accelerated proliferation of mouse myoblasts [69]. In a nanocomposite application, octadecylamine was covalently linked with NDs for imaging purposes, then mixed within a poly(lactic acid) (PLA) matrix, increasing the mechanical properties of the scaffold to that of cancellous bone [70]. Limited research has been performed on ND interactions with stem cells as well as their

capabilities in tissue engineering, in particular with their influence on hydrogel properties. However, the unique properties of NDs, including their highly modifiable surfaces and high surface area, the possibility to covalently link or adsorb therapeutics to their surface, and perhaps most significantly, their much higher biocompatibility compared to other carbon nanomaterials, should encourage further study in tissue engineering applications.

1.4 Conclusion

Despite relatively fragile mechanical properties, biocompatible and tunable biopolymer hydrogels are an active topic of research for bone tissue engineering. Filling agents, especially on the nanoscale, can add significant functionality and often increase the mechanical properties of hydrogels. The excellent biocompatibility of NDs, their hypothesized ability to enhance mechanical properties as a filling agent given the success of other carbon nanomaterials, and the ability to adsorb drugs on their surface makes them an excellent option for study in bone tissue engineering. The limited literature on NDs' interactions with stem cells and their capabilities as a filling agent in hydrogels suggests further research needs to be done to demonstrate and evaluate their potential. This project was envisioned as an exploration of that potential, while holding several possible future applications in mind. As an initial proof of concept, we aimed to explore the effect of NDs as a filling agent and therapeutic deliverer. We chose both a widely used, well-characterized hydrogel (GelMA) as well as a model osteoinductive drug (dexamethasone) to elucidate the effectiveness of NDs to simultaneously modify GelMA physical and mechanical properties while also delivering a drug. In the following chapter, we present the capabilities of NDs to adsorb dexamethasone, modulate GelMA mechanical properties, and finally, induce osteogenic differentiation via dexamethasone release to encapsulated adipose-derived mesenchymal stem cells.

Chapter 2

Gelatin-Nanodiamond Hydrogel for Drug Delivery and Bone Tissue Engineering

2.1 Abstract

Nanodiamonds (NDs), carbon-based nanoparticles typically between 4-5 nm, have attracted interest for biomedical applications due to their high surface area for adsorption and delivery of therapeutics, their modifiable surfaces, and their low toxicity. Research into the medical applications of NDs has largely focused on systemic administration of NDs, particularly for targeting tumors; thus, their integration into tissue engineering scaffolds and interactions with stem cells remains largely unexplored. Here, we report the synthesis of a nanocomposite hydrogel composed of NDs and gelatin methacrylamide (GelMA) to explore the physical and mechanical effects of NDs as a filling agent in addition to their well-known drug loading capabilities. Combining these two materials creates a flexible tissue engineering platform enabling the investigation of ND-drug complexes in 3D culture. To demonstrate these capabilities, we assess the potential of NDs to load dexamethasone within the GelMA network for the purposes of osteogenic differentiation of human adipose-derived stem cells (hASCs). We found that dexamethasone was readily loaded onto the NDs, and verified that this complex was capable of releasing the drug to hASCs *in vitro*. Inclusion of NDs within GelMA hydrogels nearly doubled the compressive strength of the hydrogels in the 2 mg/mL group, while the physical properties of the hydrogels were minimally changed. Integrating the ND-Dexamethasone complex within GelMA hydrogels resulted in successful osteogenic differentiation of encapsulated hASCs, as measured by alkaline phosphatase activity, calcium deposition, and osteocalcin expression.

2.2 Introduction

Nanocomposite hydrogels have recently become an attractive subject of study for tissue engineering applications. Hydrogels themselves, in particular those composed of biopolymers like collagen, hyaluronic acid, and alginate, exhibit properties similar to native extracellular matrix (ECM) and as a result display stellar biocompatibility along with excellent cellular adhesion and mobility [71, 72]. As a result, cells encapsulated within hydrogels show high viability and hydrogel properties can even dictate stem cell behavior and differentiation [73]. One such naturally derived hydrogel system is gelatin methacrylamide (GelMA) which has shown excellent cellular motility, adhesion, and proliferation in many previous studies and allows for the formation of complex micropatterned and 3D-printed structures as a photocrosslinkable polymer [42, 74].

In addition, GelMA has been used as a starting system for the synthesis of nanocomposite hydrogels. By using nanomaterials as filling agents to generate nanocomposites, researchers are able to create new properties for their scaffolds. Commonly, nanomaterials can modulate gel physical properties, enhance their mechanical properties, and allow more opportunities for cellular adhesion and proliferation with their high surface area:volume ratio [75]. In addition, certain nanomaterials are capable of loading therapeutics through covalent linking, electrostatic interactions, or physisorption [76].

Carbon nanomaterials, in particular graphene, single- and multi-walled carbon nanotubes (CNTs), and nanodiamonds (NDs) have garnered significant attention by biomedical researchers due to their unique mechanical, electrical, and optical properties. Both multi-walled CNTs and graphene have been shown to influence stem cell fate when integrated into tissue engineering scaffolds [77, 78], while NDs have been more limited in this area. All three of these materials have also been extensively explored for modifying intravenous drug delivery systems, given

their high surface area and functionality [76, 79]. In particular, NDs now boast a huge variety of surface functionalizations and synthesis techniques to create iterations such as carboxylated NDs, amine-functionalized NDs, and fluorescent NDs, among many others [64]. This tailoring has allowed researchers to demonstrate drug delivery of a variety of therapeutics, including small molecules [67, 80], proteins [69, 81], and nucleic acids [68, 82].

NDs have also been shown to be an effective filling agent in several studies. One report of their integration into a poly(L-lactic acid) non-hydrated porous scaffold improved the compressive strength of the scaffold to near that of cancellous bone [70]. Despite their efficacy as drug delivery vehicles, NDs remain underexplored for tissue engineering applications, especially with regards to nanocomposite hydrogels. Their demonstrated drug delivery capabilities, coupled with their significantly higher biocompatibility compared to the other carbon nanomaterials, necessitates further study in this field. We hypothesized that NDs could both effectively load and deliver a small molecule drug, dexamethasone (Dex), and add compressive strength to a conventional hydrogel, GelMA, for potential application as a bone tissue engineering scaffold. Dex is a glucocorticoid that is used clinically as an anti-inflammatory medication, but is also regularly utilized to induce osteogenic differentiation of mesenchymal stem cells (MSCs) by mediating an increase in the number of focal adhesions and intracellular tension, which in turn increases RUNX2 expression along with related osteogenic genes [83].

The goal of this study was to investigate the potential of NDs as nanofillers for influencing the properties of GelMA hydrogels and as drug-loading agents within GelMA hydrogels for 3D bone tissue engineering. We investigate the biocompatibility of NDs and their ability to load dexamethasone (Dex) and interact with human adipose-derived mesenchymal

stem cells (hASCs), as well as the mechanical and physical effects of NDs on GelMA networks. Finally, we present successful 3D osteogenic differentiation of hASCs encapsulated within GelMA/ND-Dex nanocomposite hydrogels.

2.3 Materials and Methods

2.3.1 ND Characterization and Dexamethasone Loading

To verify and quantify Dex (Sigma-Aldrich, USA) loading on the NDs (NanoAmor, USA), a dispersed ND suspension (2 mg/mL) was prepared in ethanol by sonication for 30 minutes and subsequently mixed with in equal volume with a solution of dexamethasone-fluorescein isothiocyanate (Dex-FITC) in ethanol (0.2 mg/mL) (Invitrogen, USA). Ethanol was chosen as a solvent to ensure full solubility of Dex-FITC throughout the study.

A final suspension containing 1 mg/mL of ND and 0.1 mg/mL Dex-FITC was vortexed for five minutes to ensure thorough mixing of the suspension components. Visible spectra in the range of 400-600 nm was recorded for the complex prior to centrifugation. In addition, a solution of 0.1 mg/mL Dex-FITC and a suspension of 1 mg/mL NDs were prepared as controls and their UV-Vis spectra were recorded as well. All the samples were then centrifuged for 20 minutes at 14,000 rpm. The supernatants were collected and their UV-Vis spectra recorded in the same range as stated above. Loading percentage was evaluated comparing the absorbance of Dex-FITC prior and after centrifugation of the complex at 590 nm using the following equation: $100 - (C_{post} / C_{pre}) * 100$.

2.3.2 hASC Cell Culture and ND-Dex Interactions with hASC

Human adipose-derived stem cells (hASCs) were purchased from RoosterBio (USA) and maintained in α-MEM (Invitrogen, USA) with 15% FBS (v/v) and 1% penicillin/streptomycin (v/v) at 37 °C and 5% CO_2. For differentiation studies, all cells used were in passage 3-5.

Several concentrations of NDs (10, 25, 50, 100, and 200 μg/mL) were added to hASCs in 2D culture, after which a 12 hour MTT Assay was performed according to the manufacturer's protocol (ATCC, USA) along with Calcein-AM staining (Invitrogen, USA). For apoptosis gene expression, hASCs were cultured in a 24-well plate with 500 μL complete media containing 50 μL of either UP water as a negative control, 25 μg/mL NDs in UP water, or 50 μM camptothecin (Sigma-Aldrich, USA) as a positive control. After incubation for 12 hours, gene expression was analyzed using the RT-qPCR procedure detailed below.

For observing ND-Dex interactions with hASCs, ND-Dex suspensions were prepared in ethanol, centrifuged for 20 minutes at 14,000 rpm, then resuspended in UP water and deposited onto hASCs in 500 μL complete media to a final concentration of 25 μg/mL ND and 1 μM Dex. Control groups were formulated in the same fashion using either UP water alone, 25 μg/mL NDs, or 1 uM Dex. Gene expression for Dex-related markers was then evaluated at 1 and 6 hours Dex exposure using the RT-qPCR procedure detailed below.

Both apoptosis and dexamethasone exposure qPCR studies, mRNA from each group were first extracted using an RNeasy Mini Kit (Qiagen, Germany). mRNA concentrations were measured using a NanoDrop (Thermo Scientific, USA), then normalized (100 ng mRNA) for conversion to cDNA. mRNA solutions were converted to cDNA using the High-Capacity cDNA Conversion Kit (Applied Biosystems, USA). For qPCR, all primers used were predesigned KiCqStart SYBR Green primers (Sigma-Aldrich, USA). KiCqStart SYBR Green Master Mix was used for each reaction (Sigma-Aldrich, USA). All qPCR reactions were performed using a Mastercycler Realplex^4 (Eppendorf, Germany). Fold expression levels were calculated using the $\Delta\Delta C_t$ method, using GAPDH as the housekeeping gene.

2.3.3 Immunocytochemistry

hASCs were seeded onto chamber slides, allowed to adhere and grow in complete media, then serum starved for 48 hours. ND-Dex, NDs, Dex, and UP Water were added to hASCs in the same fashion as described in section 2.3.2 and allowed to incubate for 24 hours. Cells were then fixed in 4% paraformaldehyde for 5 minutes at 37 °C, permeabilized with 0.3% Triton-X100 for 10 minutes at room temperature, then blocked with 5% normal goat serum for 45 minutes at room temperature. Mouse anti-human paxillin antibody (1:400 with 1% goat serum, Invitrogen, USA) was added to cells and left overnight at 4 °C. Goat anti-mouse AlexaFluor 594 (1:500, 1% goat serum) was then added and left for one hour at room temperature. Diamidino-2-phenylindole dilactate (DAPI, Invitrogen, USA) and phalloidin-AlexaFluor488 (Invitrogen, USA) were used to counterstain nuclei and F-actin, respectively. For staining of osteocalcin in the differentiation study, nanocomposites containing hASCs in osteoconductive media after 21 days were fixed, permeabilized, and blocked as above, then stained with mouse anti-human osteocalcin antibody (1:100 with 1% goat serum) and goat anti-mouse AlexaFluor 594 (1:500, 1% goat serum).

2.3.4 Synthesis of Gelatin Methacrylamide and GelMA/ND Nanocomposites

Gelatin A (300 g bloom from porcine skin) and methacrylic anhydride were purchased from Sigma-Aldrich (USA). GelMA was synthesized as previously described [84]. Briefly, a 10% gelatin (w/v) solution prepared in PBS at pH 7.4 was heated to 60 °C. 8 mL of methacrylic anhydride was added dropwise to methacrylate amine groups along the gelatin backbones. The polymeric mixture was stirred vigorously and maintained at 60 °C for two hours to complete the reaction, then terminated by addition of 100 mL PBS. The prepared solution was then transferred to dialysis membranes (~12-14 kDa cutoff) and dialyzed with UP water for one week with two

daily water changes. The GelMA solution was then frozen at -80 °C and lyophilized for 72 hours.

To prepare the nanocomposite hydrogels, ND suspensions of 4 mg/mL were prepared by sonication in UP water for 30 minutes. After appropriate dilutions, ND suspensions were mixed with a 14% GelMA and 0.5% photoinitiator (PI) (Irgacure 2959, Sigma-Aldrich) prepolymer solution prepared in UP water to prepare final prepolymer solutions of 7% GelMA, 0.25% PI, and ND (0, 0.5, 1, and 2 mg/mL). Prepolymer solutions were then UV crosslinked (320-500 nm) (Omnicure S200, Lumen Dynamics, Canada) for six minutes at an intensity of 7 mW/cm^2.

2.3.5 Physical and Mechanical Characterization of GelMA/ND Nanocomposites

In order to determine the swelling ratio, gels (n=5) for each group (0, 0.5, 1, and 2 mg/mL ND) were created, then frozen at -80 °C then lyophilized for 24 hours. Gels were swollen in PBS at 37 °C. After dabbing on a KimWipe to remove excess water, gel weight was measured and compared to the dry weight [(Wet weight – dry weight)/dry weight) x 100] after 1, 4, 8, 24, 48, and 72 hours.

For all mechanical studies, nanocomposites were first swollen in PBS for 24 hours. Mechanical analysis of the nanocomposites was performed using an RSA-III dynamic mechanic analyzer (TA Instruments, USA) and an AR 2000 rheometer (TA Instruments, USA). Nanocomposite cylinders (n=5) with radius 4 mm and height 2 mm were uniaxially compressed at a rate of 0.05 mm/s to obtain stress vs. strain plots from which the compressive elastic moduli were calculated using the linear portion of the curve (1-10% strain). For rheological analysis, cylindrical gels with 15 mm diameter and 4 mm height were used. Frequency sweeps were carried out from 0.01 to 10 Hz at 10% strain (in the viscoelastic region) and strain sweeps were performed from 1% to 100% strain at 1 Hz. All rheological analyses were carried out at 37 °C.

2.3.6 Micropatterning of GelMA/ND Nanocomposites

GelMA micropatterns were created using previously established procedures [74, 85]. Prior to cell encapsulation, glass slides were treated with 3-tri(methoxysilyl)propyl methacrylate (TMSPMA) (Sigma, USA). TMSPMA-coated slides were then coated with a 50 μm layer of polyethylene glycol diacrylate (PEGDA, Mw 1000 Da) (Sigma-Aldrich, USA) by UV crosslinking for 60 s. To prepare cell-laden micropatterns, hASCs were mixed with a 7% (w/v) GelMA pre-polymer solution containing 1 mg/mL of ND and 0.5% of PI. Cells were mixed in a cell density of 1.0 x 10^6 cells/mL of GelMA solution. A 45 μl of pre-polymer solution was then dropped on a petri-dish in between two spacers with a desirable height of 100 μm.

Subsequently, the PEGDA coated glass slides were placed on top of the pre-polymeric solution to obtain the aforementioned thickness. Finally, a 1x1 cm photomask was positioned on the glass slide and the entire construct was exposed to UV light (7 mW/cm^2 intensity) for 45 s. The PEGDA-coated glass slides containing patterned, crosslinked hydrogel constructs were submerged into warm DPBS. Following encapsulation, constructs were cultured in 6-well cell culture plates and supplemented with complete media. hASCs were stained using calcein-AM at 5 and 10 days according to the manufacturer's protocol (Invitrogen) and images were taken using a fluorescence microscope (Zeiss).

2.3.7 Dex-FITC Release Study

Lyophilized GelMA was mixed in PBS with 0.1% (w/v) PI to obtain a final GelMA concentration of 7% (w/v). Dex-FITC was mixed in the GelMA mixture at the concentration of 250 μg/mL. Nanocomposite hydrogels (1 mg/mL) were similarly fabricated containing the same amount of Dex-FITC. The amount of Dex-FITC released over time was determined by measuring the amount of drug not bound and washed away from the hydrogels. Briefly, 40 μL of

each GelMA/Dex-FITC mixture was placed in 96-well plates and crosslinked at 7 mW/cm^2 for 60 s. All wells were then filled with 200 μL of PBS and replaced with fresh PBS every hour for the first 8 hours and subsequently every 24 hours until a plateau was reached. The 96-well plates were protected from light and the PBS incubation solution was transferred to a new well plate. The fluorescence intensity was measured at 493 nm excitation and 519 nm emission wavelengths in a Cytation 5 plate reader (BioTek, USA). The amount of Dex-FITC was quantified using a standard calibration curve in the range of 0.4 μg/mL to 18 μg/mL. The percent of Dex-FITC release was reported as the average ± deviation standard of 4 different samples.

2.3.8 3D *In Vitro* Biocompatibility and Osteogenic Differentiation Studies

To encapsulate the hASCs into the nanocomposites, hASCs pellets were resuspended in each nanocomposite (0, 0.5, 1, and 2 mg/mL ND) prepolymer solution for a final concentration of 1 million cells/mL. Prepolymer solutions were then UV crosslinked at 7 mW/cm^2 for 60 seconds. Biocompatibility studies were carried out using an MTT assay and calcein-AM (Invitrogen, USA) staining at 72 hours, both according to the manufacturer's protocol.

For differentiation studies, hASCs (1 million cells/mL) were encapsulated as above within GelMA containing etiher 0 mg/mL ND, 1 mg/mL ND, 1 mg/mL ND and 1 μM Dex, or only 1 μM Dex. Cells were cultured in complete media for the first 48 hours after seeding, then osteoconductive media containing 50 μM ascorbic acid and 10 mM β-glycerophosphate for the remainder of the study. ALP activity at 14 days was quantified by *p*-nitrophenyl phosphate (pNPP) colorimetric assay (Sigma-Aldrich, USA) then normalized to DNA content. DNA content was determined using a PicoGreen kit (Invitrogen, USA). Briefly, nanocomposites were rinsed in PBS, lysed with lysis buffer, freeze-thawed once, sonicated, then centrifuged at 8,000 rpm for 10 minutes. The DNA content of the supernatant was then quantified. For Alizarin Red S

staining, at 14 and 21 days, cells were fixed in 4% paraformaldehyde, washed with PBS three times, then incubated with 2% Alizarin Red S (Sigma) for 20 minutes. After washing with PBS three times to remove any excess stain, brightfield images of the nanocomposites were taken. Calcium in each nanocomposite group was quantified by first determining the wet weight of each gel then freezing and lyophilizing the samples. The nanocomposites were then allowed to vortex overnight in 0.5 M hydrochloric acid for homogenization. The resulting supernatants were analyzed for calcium content via a colorimetric assay (Sigma-Aldrich, USA) per the manufacturer's protocol, then normalized to the wet weight of the hydrogel (μg/mg).

2.3.9 Statistical Analysis

Quantitative results are presented as mean ± standard deviation (SD) from independent experiments. Statistics were performed using a one-way ANOVA with a Tukey's *post hoc* test. A p value of < 0.05 was considered significant.

2.4 Results

2.4.1 Dex Loading on NDs

NDs have previously been shown to load poorly water soluble drugs, like Dex, through several theorized mechanisms [86]. To evaluate NDs' potential to load Dex, we analyzed centrifuged complexes by FTIR and EDX analysis. FTIR spectroscopy confirmed the presence of carbonyl groups (1714 cm^{-1}, ν C=O), hydroxyl groups (3421 cm^{-1}, ν O-H) and alkyl groups (2917 cm^{-1}, ν C-H) on the NDs (Figure 2.1). After centrifugation of a 10:1 ND:Dex (w/w) suspension, FTIR analysis of the resulting pellet showed characteristic peaks of Dex (1705 cm^{-1}, ν C=O; 1658 cm^{-1} and 1618 cm^{-1}, ν C=C) in the complex (Figure 2.1). TEM/EDX analysis showed a thoroughly dispersed suspension with NDs of ~5 nm diameter and confirmed the

presence of oxygen (Figure 2.2). TEM/EDX analysis of the ND-Dex pellet revealed fluorine in the complex, which was absent from the TEM/EDX of NDs (Figure 2.2).

For hASC differentiation studies, proper dosing of Dex required a quantitative assessment of loading. Because of the broad UV absorbance of NDs which overlaps with the absorbance profile of Dex, we chose to use Dex-FITC for quantitative loading studies due to its characteristic absorbace peak outside of the UV range. UV-Vis spectroscopy analysis of 10:1 ND:Dex-FITC pre- and post- spindown suspensions yielded a loading percentage of 65 ± 3% (Figure 2.3). However, it is important to note that FITC is a large addition to Dex that certainly contributes to loading in numerous ways. Because the surfaces of the NDs contain a mixture of functional groups, we theorize that a mix between hydrogen bonding, dipole-dipole interactions with surface oxygen groups, physisorption, and hydrophobic effects are responsible for the formation of the complex.

2.4.2 ND-Dex Interactions with hASCs

We next investigated the capability of the NDs to interact with the hASCs as well as deliver and release Dex. To confirm successful Dex delivery to the cells, we quantified several related genes. Serum/glucocorticoid regulated kinase 1 (SGK1) overexpression was recently identified as the first step in osteogenic differentiation of MSCs due to Dex exposure [87]. After incubation for one hour with a centrifuged then resuspended ND-Dex pellet, hASCs showed significantly higher expression of SGK1 compared to resuspended NDs and a negative control containing no NDs or Dex (Figure 2.4). MSCs are also known to produce more integrin α5 and β1 (ITGA5, ITGB1) as well as increase extracellular deposition of fibronectin for integrin α5β1 anchoring [88]. Accordingly, ND-Dex exposure for six hours significantly increased ITGA5 expression compared to controls (Figure 2.4). Increased focal adhesion stability leads to a higher

number of focal adhesions upon Dex exposure. Immunostain of paxillin (PXN), a protein which participates in focal adhesion activity by binding to β-integrin cytoplasmic domains, was observed to be more extensive in hASCs in response to both ND-Dex and Dex (Figure 2.5).

2.4.3 Physical and Mechanical Characterization of GelMA/ND Nanocomposites

GelMA/ND nanocomposites (NCs) at concentrations of 0.5, 1, and 2 mg/mL were fabricated and characterized. SEM images of both GelMA and 2 mg/mL GelMA-ND gels revealed similar interconnected porous networks in all groups. (Figure 2.7). The swelling ratio, crucial to determine the ability of hydrogels to exchange waste and nutrients with surrounding fluid, was measured in PBS at pH 7.4 at 37 °C. No significant differences were seen between GelMA and 2 mg/mL GelMA-ND at each swelling time point (Figure 2.7). Similar swelling ratios between the two systems corroborates the similar porosity seen in the SEM images.

Elastic moduli steadily increased with addition of NDs to the GelMA network, with 2 mg/mL nearly doubling the modulus of GelMA alone as well as being significantly higher than 0.5 mg/mL nanocomposites (Figure 2.8). Given these results, we focused on GelMA and the 2 mg/mL system for the remaining mechanical studies. Ultimate fracture strength (UCS) was reached at ~80% strain for GelMA and 2 mg/mL nanocomposites and the presence of the NDs again nearly doubled the UCS (~260 kPa vs. ~180 kPa) in representative samples (Figure 2.8). The rheology of the gels, as measured by an oscillatory frequency sweep, also changed significantly for the 2 mg/mL nanocomposites compared to the GelMA (Figure 2.8). Both the storage (G') and loss (G'') moduli were increased for all frequencies tested upon addition of NDs. The frequency sweeps in both cases showed G' and G'' curves consistent with highly crosslinked gels, in which G' and G'' both remained stable up until the final frequency, with very little variation throughout the test.

2.4.4 ND and GelMA-ND Biocompatibility Studies

Extensive evaluation of nanomaterial biocompatibility is crucial for determining their suitability for drug delivery and cellular uptake. Thus, we proceeded with a more thorough investigation of ND biocompatibility with hASCs. qPCR analysis revealed no difference in the expression of a variety of pro- and anti-apoptotic genes when hASCs were exposed to NDs for 12 hours (Figure 2.6). Likewise, concentrations of NDs ranging from 10-100 µg/mL showed no significant reduction in viability and proliferation in an MTT assay (Figure 2.6).

We next tested the biocompatibility of the hASCs upon encapsulation within GelMA and the nanocomposites. Prepolymer solutions of GelMA and each ND concentration containing 1 million cells/mL, were UV crosslinked for 60 seconds to form the constructs. hASCs showed excellent viability and spindle-like morphology after 72 hours. MTT assay confirmed no significant changes in viability between hASCs encapsulated in the three ND concentrations (0.5, 1, and 2 mg/mL) as well as GelMA alone (Figure 2.9). Calcein-AM staining, again at 72 hours, showed cells adhering and stretching throughout the entire network of the GelMA and nanocomposites hydrogels (Figure 2.9).

2.4.5 Micropatterning of GelMA-ND Nanocomposites

Refining both 3D cell culture for drug discovery and mechanistic studies, as well as furthering regenerative medicine technologies, requires further control over the microstructure of constructs. GelMA has been previously used for this purpose and shows potential to create complex, ordered structures [74]. Cylindrical 1 mm micropatterns of both GelMA and 1 mg/mL nanocomposites were fabricated. Nanocomposites appeared to have more defined structure according to SEM and brightfield images. GelMA/ND nanocomposites containing 1 mg/mL NDs encapsulating 1 million hASCs/mL were successfully used to create cell-laden micropatterns.

Calcein-AM staining at 5 and 10 days showed excellent cell viability and spreading within the microgels (Figure 2.10).

2.4.6 Osteogenic Differentiation of Encapsulated hASCs within GelMA/ND-Dex

Release of Dex-FITC from nanocomposite hydrogels was significantly extended compared to GelMA controls. At 72 hours, ~50% of encapsulated Dex-FITC remained in the nanocomposites compared to less than 10% in GelMA hydrogels (Figure 2.11). These non-Fickian release kinetics can be attributed to a variety of possible interactions, such as hydrogen bonding, physisorption, and hydrophobic effect. After proving the enhanced retention of Dex in the nanocomposite hydrogels, we investigated the potential of this system to initiate osteogenic differentiation of encapsulated hASCs. The nanocomposite hydrogels containing Dex showed superior osteogenic differentiation compared to all controls as measured by ALP activity and staining, calcium deposition, and osteocalcin staining.

ALP activity, an early marker of osteogenic differentiation, increases intracellular concentrations of free phosphate by hydrolysis of pyrophosphate [89]. Both quantitative and qualitative evaluations of ALP activity were performed at 14 days. ALP activity (Figure 2.10) was increased significantly compared to all other groups in the ND-Dex group, and qualitative staining of ALP corroborated this finding (Figure 2.12). Alizarin Red S colorimetric stain allows qualitative comparison of bone-like calcium deposits. At both 14 and 21 days, all control groups showed minor mineralization, while ND-Dex showed significantly more red staining and thus calcium deposition (Figure 2.13). Finally, immunostaining for osteocalcin (OCN) provided further evidence for successful osteogenic differentiation of hASCs. OCN is an osteoblast-specific marker that serves both endocrine functions and mineralization functions. ND-Dex

nanocomposites showed increased OCN staining, while control groups displayed very little or no staining (Figure 2.14).

2.5 Discussion

Dexamethasone loading on NDs was successful as confirmed by several methods, specifically at a ratio of 10:1 ND:Dex. Other studies have shown similar results when loading small molecules onto NDs [67, 86], though the exact mechanism of loading in this case requires further investigation. Analysis of our NDs showed a heterogeneous surface chemistry composed of a mixture of carbonyl, alcohol, and alkyl groups. As a result, it is not possible to speculate as to the exact mechanism of loading, be it through hydrogen bonding, dipole-dipole interactions between Dex and carbonyl groups, physisorption by van der Waal forces, or hydrophobic effects forcing interaction between the two. Previous studies of hydrophobic drugs and ND complexation were hypothesized to be primarily due to interactions with surface carboxyl groups [86]. The several hydroxyl groups available on Dex make hydrogen bonding with surface carbonyl groups in our case a possibility; in addition, hydrophobic regions of ND surfaces can interact with hydrophobic Dex through physisorption. Further studies to determine the loading mechanism should assess the loading efficiency of a panel of NDs with varying surface functionalizations. Our quantification of loading includes the effect of FITC and thus may not be completely accurate, given that FITC is comparable to Dex in molecular weight and also contains groups capable of interacting with the ND surface.

The improvement of GelMA mechanical properties in response to ND addition was encouraging, given that other carbon nanomaterials have shown similar results both when simply added to the GelMA network [90, 91] and when covalently linked to it [92]. This revelation is particularly important in the context of UV crosslinkable gels, since NDs do absorb UV light and

certain types have even been explored as a UV protectant [93]. Interestingly, the mechanical properties showed a significant increase while no discernable changes in porosity or swelling ratio were observed upon ND addition to the network. Previous studies have shown both increases [55] and decreases [94], depending on the nanomaterial included, in porosity along with increased mechanical strength. For instance, enhanced ionic interactions between charged silica nanoparticles and amine and carboxyl groups contained in GelMA resulted in increased mechanical strength but also increased pore size [55]. The lack of physical change in our hydrogels suggests that GelMA crosslinking in this case has significantly more control over the swelling and porosity properties of the gel.

NDs are well-known to be biocompatible as measured by higher cell viability at varying concentrations and lower reactive oxygen species production compared to graphene and CNTs; however, different carbon nanomaterials have been shown to have different cytotoxicities on varying cell type [95]. As expected, the NDs showed excellent biocompatibility, both by MTT assay and qPCR studies for a variety of anti- and pro-apoptotic markers. qPCR offered a more refined look at potential sources of apoptosis or anti-apoptosis. No significant differences between the negative control and ND exposed cells were observed, further confirming the biocompatibility of NDs with hASCs. Each chosen apoptotic gene has been shown to be related to mitochondrial regulated apoptosis, which carbon nanomaterials, particularly those inducing oxidative stress, have been shown to initiate [96-98]. Much current work focuses on lysosomal and autophagic disruption as mechanisms for nanomaterial-induced apoptosis [99]; though NDs have so far shown excellent biocompatibility, investigating these sources of apoptosis could further our understanding of why NDs have less toxicity than other carbon nanomaterials.

Studies on lysosomal disruption also have important implications for ND-based drug delivery, as NDs are mostly taken up by this route.

Generally, NDs show much higher cellular uptake than other carbon nanomaterials [66] and appear to be taken up by clathrin-mediated endocytosis, with individual nanodiamonds localizing to the cytosol and larger complexes remaining in vesicles [100]. The cellular uptake, drug delivery capabilities, and biocompatibility of NDs by several cell types has been characterized, but this study is the first of our knowledge to report their capabilities with regards to stem cells. SGK1 overexpression in response to Dex increases microtubule instability, focal adhesion number and stability, and in turn intracellular tension and osteogenic gene expression [87]. Its overexpression, along with the noted cytoskeletal markers, confirmed that the ND-Dex complex was capable of delivering Dex in two possible ways: either Dex was released from ND-Dex complexes and diffused into the cell, or NDs adsorbing Dex were taken up by the cell and Dex was released therein. For 3D *in vitro* and therapeutic applications, the second mechanism would be preferable; as cells spread and move within the nanocomposites, more NDs are taken up and exposed to adsorbed Dex, while Dex release to the surrounding fluid is limited. Understanding the kinetics of ND-Dex and other drug interactions along with which of these mechanisms dominates is a crucial subject for future research. Regardless of the exact mechanism of Dex delivery to the hASCs in this study, we were able to control release of Dex by nanocomposites, and demonstrated successful osteogenic differentiation.

Chapter 3

Conclusion and Future Directions

We successfully demonstrated NDs' capabilities to load and deliver Dex, synthesized and characterized GelMA/ND nanocomposites, furthered study of the biocompatibility of NDs with mesenchymal stem cells, and finally succeeded in 3D osteogenic differentiation using the loading ability of our NDs in conjunction with GelMA. Successful loading and delivery of Dex, along with the improvement in mechanical properties of GelMA by NDs, demonstrates their potential for tissue engineering applications, encourages future studies, and also provides another example of their well-established drug delivery capabilities. However, further characterization of the NDs and Dex from this study must be performed to fully understand complexation and its influence on drug loading and release from the NDs. In order to evaluate the influence of Dex on the aggregation of NDs as well as the colloidal stability of ND-Dex complexes compared to NDs alone, we plan on performing dynamic light scattering (DLS) as well as zeta potential analysis to observe ND-Dex aggregate size and stability. In addition, though our release study did demonstrate that NDs were able to extend Dex retention within GelMA, further work can be done to postulate how this occurred. The release observed from GelMA alone appeared to be standard Fickian release, while the GelMA-ND study appeared to show a short burst release, followed by a more extended retention of Dex by the NDs. It is possible that Dex that was uncomplexed with NDs was released in short order, while complexed Dex was required to desorb from the ND surface, then release into the surrounding media. We will seek to fit different models to this release profile, which may lend insight into what the dominant mechanism of release is.

Given the success of this design, future work can be done to evaluate its *in vivo* effectiveness in a cranial defect model. An *in* vivo study will require additional work to be able to effectively deliver the hydrogel to a variety of defects of different size and shape, given that GelMA is not realistically an injectable material. We are currently evaluating the capability to 3D bioprint GelMA-ND prepolymer solutions containing hASCs. This study could also be an excellent opportunity to evaluate the potential of NDs for clinical translation from a broader perspective, with a focus on their biodistribution and potential toxicity after degradation of a hydrogel-ND scaffold. A study in parallel that uses fluorescent NDs, ideally with a similar surface chemistry, integrated into a GelMA network could enable study of biodistribution after different degradation time points. Observing the functionality and health of tissues with high ND load after implantation is crucial to tuning future clinical applications of NDs. Biodistribution studies must also include an assessment of how and if the NDs are cleared. In our application, quick clearance of both NDs that elute out of the One potential avenue of study is observation of protein adsorption, significant amounts of which can lead to quick excretion by the liver. We are interested in pairing this concept with our study on GelMA-ND degradation *in vitro*, in addition to studying it *in vivo* eventually.

As expected based on previous work with other carbon nanomaterials, NDs were able to improve the mechanical properties of GelMA through the nanofilling effect. Theoretically, NDs participate in the GelMA network via transient interactions, allowing them to bear some load upon disturbance of the network. However, given that the NDs do have sites available for free radical formation upon contact with a photoinitiator, it is possible that some NDs are able to crosslink covalently with the polymer itself. How frequently this occurs and its influence on GelMA mechanical properties is another opportunity for future study. Though NDs did improve

the strength of the GelMA network, the improvement was certainly not enough for the hydrogel to be used alone in a load-bearing application. However, discarding hydrogels such as this one for use in load-bearing defects would be unwise given their versatility and ability to mimic endochondral ossification. Thus, we are interested in the possibility of creating biphasic scaffolds by integrating this and other osteoinductive hydrogels with stronger synthetic scaffolding materials for the treatment of load-bearing defects. In particular, 3D-printed scaffolds with moderate porosity for filling with osteoinductive hydrogels might provide the mechanical strength necessary for these defects, while also having surface area available for hydrogel coating and crosslinking.

Success in this study can be expanded upon in a number of ways. Perhaps the most glaring deficiency of this study is that we took little advantage of one of the greatest assets of NDs: their tailorable surface chemistry. As previously mentioned, studies on NDs have produced many surface-functionalizations which can be utilized in tissue engineering. One concept that has been pursued with other nanomaterials, including graphene and CNTs, is covalent immobilization onto the scaffolding hydrogel. Higher increases to stiffness have been observed with this method compared to the simple filling used in this study, especially at higher nanomaterial concentration. A minor increase in compressive strength was achieved in this project, but we theorize a significantly larger one could be gained by this method, as the NDs are no longer a simple filling agent but are chemically integrated into the network. Similarly, drugs have been covalently linked to NDs to further control over release. An exciting approach would be to combine these capabilities; simultaneous linking of drug and polymer to NDs could lead to more robust hydrogels with enhanced release profiles depending on the application. We are currently exploring the possibility of a one-step reaction to link both Dex and GelMA to

functionalized NDs. Clearly, this strategy would apply beyond bone tissue engineering. For example, acid-sensitive linkages to both polymer and drug are an intriguing possibility for cancer therapy; NDs' demonstrated ability to localize to tumors and avoid drug efflux, coupled with controlled degradation and release in the tumor microenvironment may lead to an effective therapy.

Imaging with fluorescent NDs also hold intriguing possibilities in tissue engineering and bone tissue engineering. As mentioned in previous sections, an octadecylamine-functionalized NDs coating on PLLA implants allowed imaging of implants. *In vitro,* fluorescent microscale beads are frequently used for studies of cell migration and tracking. Filling hydrogels with fluorescent NDs could allow studies of cellular migration and traction in a 3D matrix, much in the same way these larger fluorescent beads can. If the distribution of fluorescent NDs could be controlled, they might allow finer tracking of cells. Where fluorescent NDs may be especially useful is in the imaging and tracking of implanted gels or implants *in vivo*; perhaps real time monitoring of drug release and degradation of the scaffold is a possibility with this tool.

References

1. Hoc, T., et al., *Effect of microstructure on the mechanical properties of Haversian cortical bone*. Bone, 2006. **38**(4): p. 466-474.
2. Bayraktar, H.H., et al., *Comparison of the elastic and yield properties of human femoral trabecular and cortical bone tissue.* Journal of Biomechanics, 2004. **37**(1): p. 27-35.
3. Tong, W., et al., *Size and shape of mineralites in young bovine bone measured by atomic force microscopy.* Calcified Tissue International, 2003. **72**(5): p. 592-598.
4. Eppell, S.J., et al., *Shape and size of isolated bone mineralites measured using atomic force microscopy.* Journal of orthopaedic research, 2001. **19**(6): p. 1027-1034.
5. Iain H. Kalfas, *Principles of bone healing.* Neurosurgical Focus, 2001. **10**(4): p. 1-4.
6. Ai-Aql, Z., et al., *Molecular mechanisms controlling bone formation during fracture healing and distraction osteogenesis.* Journal of dental research, 2008. **87**(2): p. 107-118.
7. Johnell, O. and J. Kanis, *An estimate of the worldwide prevalence and disability associated with osteoporotic fractures.* Osteoporosis international, 2006. **17**(12): p. 1726-1733.
8. Arden, N.K., et al., *Knee pain, knee osteoarthritis, and the risk of fracture.* Arthritis Care & Research, 2006. **55**(4): p. 610-615.
9. Kurtz, S.M., et al., *International survey of primary and revision total knee replacement.* International orthopaedics, 2011. **35**(12): p. 1783-1789.
10. Losina, E., et al., *The dramatic increase in total knee replacement utilization rates in the United States cannot be fully explained by growth in population size and the obesity epidemic.* J Bone Joint Surg Am, 2012. **94**(3): p. 201-207.
11. Kurtz, S.M., et al., *Impact of the Economic Downturn on Total Joint Replacement Demand in the United States.* Updated Projections to 2021, 2014. **96**(8): p. 624-630.
12. Wong, K.C. and S.M. Kumta, *Joint-preserving tumor resection and reconstruction using image-guided computer navigation.* Clinical Orthopaedics and Related Research®, 2013. **471**(3): p. 762-773.
13. Harwood, P.J., J.B. Newman, and A.L. Michael, *(ii) An update on fracture healing and non-union.* Orthopaedics and Trauma, 2010. **24**(1): p. 9-23.
14. Spicer, P.P., et al., *Evaluation of bone regeneration using the rat critical size calvarial defect.* Nature protocols, 2012. **7**(10): p. 1918-1929.
15. Silber, J.S., et al., *Donor site morbidity after anterior iliac crest bone harvest for single-level anterior cervical discectomy and fusion.* Spine, 2003. **28**(2): p. 134-139.
16. Heary, R.F., et al., *Persistent iliac crest donor site pain: independent outcome assessment.* Neurosurgery, 2002. **50**(3): p. 510-517.
17. Hou, C.-H., R.-S. Yang, and S.-M. Hou, *Hospital-based allogenic bone bank—10-year experience.* Journal of Hospital Infection, 2005. **59**(1): p. 41-45.
18. Mankin, H.J., F.J. Hornicek, and K.A. Raskin, *Infection in massive bone allografts.* Clinical orthopaedics and related research, 2005. **432**: p. 210-216.
19. Wheeler, D.L. and W.F. Enneking, *Allograft bone decreases in strength in vivo over time.* Clinical orthopaedics and related research, 2005. **435**: p. 36-42.
20. Van Heest, A. and M. Swiontkowski, *Bone-graft substitutes.* The Lancet, 1999. **353**: p. S28-S29.
21. Porter, J.R., T.T. Ruckh, and K.C. Popat, *Bone tissue engineering: A review in bone biomimetics and drug delivery strategies.* Biotechnology Progress, 2009. **25**(6): p. 1539-1560.

22. Bose, S., M. Roy, and A. Bandyopadhyay, *Recent advances in bone tissue engineering scaffolds.* Trends in biotechnology, 2012. **30**(10): p. 546-554.
23. Pina, S., J.M. Oliveira, and R.L. Reis, *Natural-Based Nanocomposites for Bone Tissue Engineering and Regenerative Medicine: A Review.* Advanced Materials, 2015. **27**(7): p. 1143-1169.
24. Gerhardt, L.-C. and A.R. Boccaccini, *Bioactive glass and glass-ceramic scaffolds for bone tissue engineering.* Materials, 2010. **3**(7): p. 3867-3910.
25. Bose, S. and S. Tarafder, *Calcium phosphate ceramic systems in growth factor and drug delivery for bone tissue engineering: a review.* Acta biomaterialia, 2012. **8**(4): p. 1401-1421.
26. Maxson, S., et al., *Concise review: role of mesenchymal stem cells in wound repair.* Stem cells translational medicine, 2012. **1**(2): p. 142-149.
27. Wang, X., et al., *Role of mesenchymal stem cells in bone regeneration and fracture repair: a review.* International orthopaedics, 2013. **37**(12): p. 2491-2498.
28. Nuttelman, C.R., M.C. Tripodi, and K.S. Anseth, *Dexamethasone-functionalized gels induce osteogenic differentiation of encapsulated hMSCs.* Journal of Biomedical Materials Research Part A, 2006. **76**(1): p. 183-195.
29. Chen, W., et al., *PDGFB-based stem cell gene therapy increases bone strength in the mouse.* Proceedings of the National Academy of Sciences, 2015. **112**(29): p. E3893-E3900.
30. Manaka, T., et al., *Local delivery of siRNA using a biodegradable polymer application to enhance BMP-induced bone formation.* Biomaterials, 2011. **32**(36): p. 9642-9648.
31. Zhang, X.-Q., et al., *Polymer-functionalized nanodiamond platforms as vehicles for gene delivery.* ACS nano, 2009. **3**(9): p. 2609-2616.
32. Annabi, N., et al., *Controlling the porosity and microarchitecture of hydrogels for tissue engineering.* Tissue Engineering Part B: Reviews, 2010. **16**(4): p. 371-383.
33. Cui, W., Y. Zhou, and J. Chang, *Electrospun nanofibrous materials for tissue engineering and drug delivery.* Science and Technology of Advanced Materials, 2016.
34. Zhao, L., M.D. Weir, and H.H.K. Xu, *An injectable calcium phosphate-alginate hydrogel-umbilical cord mesenchymal stem cell paste for bone tissue engineering.* Biomaterials, 2010. **31**(25): p. 6502-6510.
35. Wang, L. and J.P. Stegemann, *Thermogelling chitosan and collagen composite hydrogels initiated with β-glycerophosphate for bone tissue engineering.* Biomaterials, 2010. **31**(14): p. 3976-3985.
36. Burdick, J.A. and G.D. Prestwich, *Hyaluronic Acid Hydrogels for Biomedical Applications.* Advanced Materials, 2011. **23**(12): p. H41-H56.
37. Patterson, J., et al., *Hyaluronic acid hydrogels with controlled degradation properties for oriented bone regeneration.* Biomaterials, 2010. **31**(26): p. 6772-6781.
38. Perez, R.A., et al., *Porous hydroxyapatite and gelatin/hydroxyapatite microspheres obtained by calcium phosphate cement emulsion.* Journal of Biomedical Materials Research Part B: Applied Biomaterials, 2011. **97**(1): p. 156-166.
39. Quinlan, E., et al., *Development of collagen–hydroxyapatite scaffolds incorporating PLGA and alginate microparticles for the controlled delivery of rhBMP-2 for bone tissue engineering.* Journal of Controlled Release, 2015. **198**: p. 71-79.
40. Kloxin, A.M., et al., *Mechanical properties of cellularly responsive hydrogels and their experimental determination.* Advanced materials, 2010. **22**(31): p. 3484-3494.

41. Kloxin, A.M., et al., *Tunable hydrogels for external manipulation of cellular microenvironments through controlled photodegradation.* Advanced Materials, 2010. **22**(1): p. 61-66.
42. Yue, K., et al., *Synthesis, properties, and biomedical applications of gelatin methacryloyl (GelMA) hydrogels.* Biomaterials, 2015. **73**: p. 254-271.
43. Huh, D., G.A. Hamilton, and D.E. Ingber, *From 3D cell culture to organs-on-chips.* Trends in cell biology, 2011. **21**(12): p. 745-754.
44. Tibbitt, M.W. and K.S. Anseth, *Hydrogels as extracellular matrix mimics for 3D cell culture.* Biotechnology and Bioengineering, 2009. **103**(4): p. 655-663.
45. Bertassoni, L.E., et al., *Hydrogel bioprinted microchannel networks for vascularization of tissue engineering constructs.* Lab on a Chip, 2014. **14**(13): p. 2202-2211.
46. Qi, H., et al., *Patterned differentiation of individual embryoid bodies in spatially organized 3D hybrid microgels.* Advanced materials, 2010. **22**(46): p. 5276-5281.
47. Docherty-Skogh, A.-C., et al., *Bone morphogenetic protein-2 delivered by hyaluronan-based hydrogel induces massive bone formation and healing of cranial defects in minipigs.* Plastic and reconstructive surgery, 2010. **125**(5): p. 1383-1392.
48. Szpalski, C., et al., *Cranial bone defects: current and future strategies.* Neurosurgical focus, 2010. **29**(6): p. E8.
49. Yang, L., et al., *Hypertrophic chondrocytes can become osteoblasts and osteocytes in endochondral bone formation.* Proceedings of the National Academy of Sciences, 2014. **111**(33): p. 12097-12102.
50. Thompson, E.M., et al., *An Endochondral Ossification-Based Approach to Bone Repair: Chondrogenically Primed Mesenchymal Stem Cell-Laden Scaffolds Support Greater Repair of Critical-Sized Cranial Defects Than Osteogenically Stimulated Constructs In Vivo.* Tissue Engineering Part A, 2016. **22**(5-6): p. 556-567.
51. Visser, J., et al., *Endochondral bone formation in gelatin methacrylamide hydrogel with embedded cartilage-derived matrix particles.* Biomaterials, 2015. **37**: p. 174-182.
52. Thompson, E.M., et al., *Recapitulating endochondral ossification: a promising route to in vivo bone regeneration.* Journal of Tissue Engineering and Regenerative Medicine, 2015. **9**(8): p. 889-902.
53. Pola, R., et al., *The morphogen Sonic hedgehog is an indirect angiogenic agent upregulating two families of angiogenic growth factors.* Nature medicine, 2001. **7**(6): p. 706-711.
54. Rivron, N.C., et al., *Sonic Hedgehog-activated engineered blood vessels enhance bone tissue formation.* Proceedings of the National Academy of Sciences, 2012. **109**(12): p. 4413-4418.
55. Xavier, J.R., et al., *Bioactive nanoengineered hydrogels for bone tissue engineering: a growth-factor-free approach.* ACS nano, 2015. **9**(3): p. 3109-3118.
56. Gaharwar, A.K., et al., *Photocrosslinked nanocomposite hydrogels from PEG and silica nanospheres: structural, mechanical and cell adhesion characteristics.* Materials Science and Engineering: C, 2013. **33**(3): p. 1800-1807.
57. Fu, S., et al., *Injectable and thermo-sensitive PEG-PCL-PEG copolymer/collagen/n-HA hydrogel composite for guided bone regeneration.* Biomaterials, 2012. **33**(19): p. 4801-4809.
58. Nayak, T.R., et al., *Graphene for controlled and accelerated osteogenic differentiation of human mesenchymal stem cells.* ACS nano, 2011. **5**(6): p. 4670-4678.

59. Park, S.Y., et al., *Enhanced differentiation of human neural stem cells into neurons on graphene.* Advanced Materials, 2011. **23**(36).
60. Park, J., et al., *Graphene–Regulated Cardiomyogenic Differentiation Process of Mesenchymal Stem Cells by Enhancing the Expression of Extracellular Matrix Proteins and Cell Signaling Molecules.* Advanced healthcare materials, 2014. **3**(2): p. 176-181.
61. La, W.G., et al., *Delivery of a therapeutic protein for bone regeneration from a substrate coated with graphene oxide.* Small, 2013. **9**(23): p. 4051-4060.
62. Li, X., et al., *The use of carbon nanotubes to induce osteogenic differentiation of human adipose-derived MSCs in vitro and ectopic bone formation in vivo.* Biomaterials, 2012. **33**(19): p. 4818-4827.
63. Venkatesan, J., et al., *Preparation and characterization of carbon nanotube-grafted-chitosan – Natural hydroxyapatite composite for bone tissue engineering.* Carbohydrate Polymers, 2011. **83**(2): p. 569-577.
64. Mochalin, V.N., et al., *The properties and applications of nanodiamonds.* Nat Nano, 2012. **7**(1): p. 11-23.
65. Krueger, A. and D. Lang, *Functionality is key: recent progress in the surface modification of nanodiamond.* Advanced Functional Materials, 2012. **22**(5): p. 890-906.
66. Zhang, X., et al., *A comparative study of cellular uptake and cytotoxicity of multi-walled carbon nanotubes, graphene oxide, and nanodiamond.* Toxicology Research, 2012. **1**(1): p. 62-68.
67. Chow, E.K., et al., *Nanodiamond Therapeutic Delivery Agents Mediate Enhanced Chemoresistant Tumor Treatment.* Science Translational Medicine, 2011. **3**(73): p. 73ra21-73ra21.
68. Alhaddad, A., et al., *Nanodiamond as a vector for siRNA delivery to Ewing sarcoma cells.* Small, 2011. **7**(21): p. 3087-3095.
69. Moore, L., et al., *Multi-protein delivery by nanodiamonds promotes bone formation.* Journal of dental research, 2013: p. 0022034513504952.
70. Zhang, Q., et al., *Fluorescent PLLA-nanodiamond composites for bone tissue engineering.* Biomaterials, 2011. **32**(1): p. 87-94.
71. Van Vlierberghe, S., P. Dubruel, and E. Schacht, *Biopolymer-based hydrogels as scaffolds for tissue engineering applications: a review.* Biomacromolecules, 2011. **12**(5): p. 1387-1408.
72. Swetha, M., et al., *Biocomposites containing natural polymers and hydroxyapatite for bone tissue engineering.* International journal of biological macromolecules, 2010. **47**(1): p. 1-4.
73. Trappmann, B., et al., *Extracellular-matrix tethering regulates stem-cell fate.* Nature materials, 2012. **11**(7): p. 642-649.
74. Nichol, J.W., et al., *Cell-laden microengineered gelatin methacrylate hydrogels.* Biomaterials, 2010. **31**(21): p. 5536-5544.
75. Gaharwar, A.K., N.A. Peppas, and A. Khademhosseini, *Nanocomposite hydrogels for biomedical applications.* Biotechnology and Bioengineering, 2014. **111**(3): p. 441-453.
76. Goenka, S., V. Sant, and S. Sant, *Graphene-based nanomaterials for drug delivery and tissue engineering.* Journal of Controlled Release, 2014. **173**: p. 75-88.
77. Akhavan, O., E. Ghaderi, and M. Shahsavar, *Graphene nanogrids for selective and fast osteogenic differentiation of human mesenchymal stem cells.* Carbon, 2013. **59**: p. 200-211.

78. Namgung, S., et al., *Controlling the growth and differentiation of human mesenchymal stem cells by the arrangement of individual carbon nanotubes.* Acs Nano, 2011. **5**(9): p. 7383-7390.
79. Mochalin, V.N., et al., *The properties and applications of nanodiamonds.* Nature nanotechnology, 2012. **7**(1): p. 11-23.
80. Liu, K.-K., et al., *Covalent linkage of nanodiamond-paclitaxel for drug delivery and cancer therapy.* Nanotechnology, 2010. **21**(31): p. 315106.
81. Shimkunas, R.A., et al., *Nanodiamond–insulin complexes as pH-dependent protein delivery vehicles.* Biomaterials, 2009. **30**(29): p. 5720-5728.
82. Cao, N., et al., *The synergistic effect of hierarchical assemblies of siRNA and chemotherapeutic drugs co-delivered into hepatic cancer cells.* Biomaterials, 2011. **32**(8): p. 2222-2232.
83. Hamidouche, Z., et al., *FHL2 mediates dexamethasone-induced mesenchymal cell differentiation into osteoblasts by activating Wnt/β-catenin signaling-dependent Runx2 expression.* The FASEB Journal, 2008. **22**(11): p. 3813-3822.
84. Van Den Bulcke, A.I., et al., *Structural and rheological properties of methacrylamide modified gelatin hydrogels.* Biomacromolecules, 2000. **1**(1): p. 31-38.
85. Du, Y., et al., *Directed assembly of cell-laden microgels for fabrication of 3D tissue constructs.* Proceedings of the National Academy of Sciences, 2008. **105**(28): p. 9522-9527.
86. Chen, M., et al., *Nanodiamond-Mediated Delivery of Water-Insoluble Therapeutics.* ACS Nano, 2009. **3**(7): p. 2016-2022.
87. Wang, H.-L., et al., *Dexamethasone-induced cellular tension requires a SGK1-stimulated Sec5–GEF-H1 interaction.* Journal of Cell Science, 2015. **128**(20): p. 3757-3768.
88. Hamidouche, Z., et al., *Priming integrin α5 promotes human mesenchymal stromal cell osteoblast differentiation and osteogenesis.* Proceedings of the National Academy of Sciences, 2009. **106**(44): p. 18587-18591.
89. Orimo, H., *The mechanism of mineralization and the role of alkaline phosphatase in health and disease.* Journal of Nippon Medical School, 2010. **77**(1): p. 4-12.
90. Shin, S.R., et al., *Carbon-nanotube-embedded hydrogel sheets for engineering cardiac constructs and bioactuators.* ACS nano, 2013. **7**(3): p. 2369-2380.
91. Shin, S.R., et al., *Cell-laden Microengineered and Mechanically Tunable Hybrid Hydrogels of Gelatin and Graphene Oxide.* Advanced Materials, 2013. **25**(44): p. 6385-6391.
92. Cha, C., et al., *Controlling Mechanical Properties of Cell-Laden Hydrogels by Covalent Incorporation of Graphene Oxide.* Small, 2014. **10**(3): p. 514-523.
93. Shenderova, O., et al., *Detonation nanodiamonds as UV radiation filter.* Diamond and Related Materials, 2007. **16**(12): p. 2003-2008.
94. Wang, Q., et al., *Super-tough double-network hydrogels reinforced by covalently compositing with silica-nanoparticles.* Soft Matter, 2012. **8**(22): p. 6048-6056.
95. Sohaebuddin, S.K., et al., *Nanomaterial cytotoxicity is composition, size, and cell type dependent.* Particle and fibre toxicology, 2010. **7**(1): p. 1.
96. Shvedova, A.A., et al., *Inhalation vs. aspiration of single-walled carbon nanotubes in C57BL/6 mice: inflammation, fibrosis, oxidative stress, and mutagenesis.* American Journal of Physiology-Lung Cellular and Molecular Physiology, 2008. **295**(4): p. L552-L565.

97. Yang, H., et al., *Comparative study of cytotoxicity, oxidative stress and genotoxicity induced by four typical nanomaterials: the role of particle size, shape and composition.* Journal of applied Toxicology, 2009. **29**(1): p. 69-78.
98. Shvedova, A.A., et al., *Mechanisms of carbon nanotube-induced toxicity: focus on oxidative stress.* Toxicology and applied pharmacology, 2012. **261**(2): p. 121-133.
99. Stern, S.T., P.P. Adiseshaiah, and R.M. Crist, *Autophagy and lysosomal dysfunction as emerging mechanisms of nanomaterial toxicity.* Particle and fibre toxicology, 2012. **9**(1): p. 1.
100. McGuinness, L.P., et al., *Quantum measurement and orientation tracking of fluorescent nanodiamonds inside living cells.* Nat Nano, 2011. **6**(6): p. 358-363.

Figures

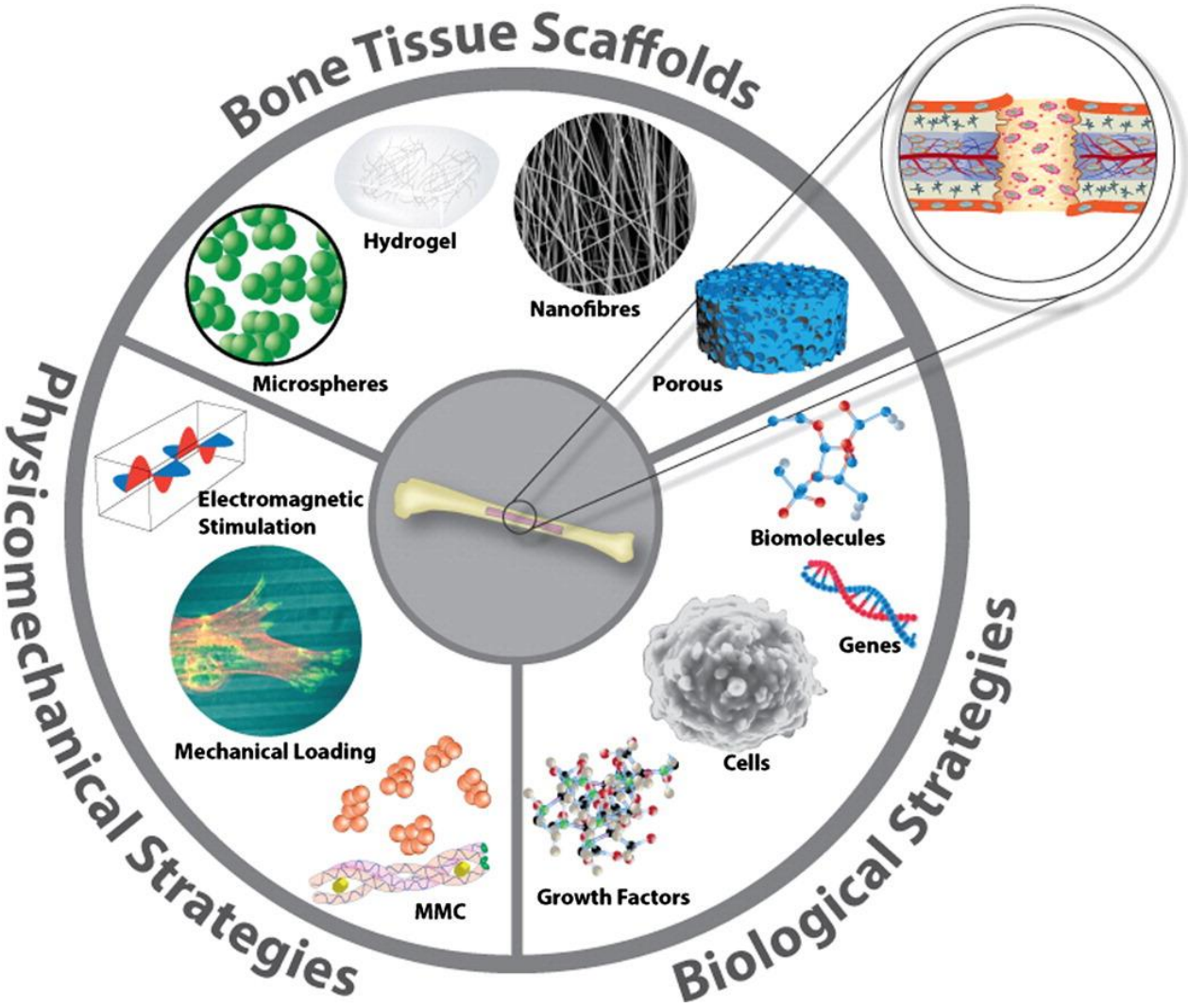

Figure 1.1

Summary of Bone Tissue Engineering Strategies. Numerous scaffolds, therapeutics, and mechanical stimulation strategies have been explored for regenerating bone tissue. Ideal scaffolds must have controlled porosity and degradation profiles, encourage vascularization of newly forming bone tissue, and enable the controlled, local delivery of cells and drugs. (Reprinted from *Advanced Drug Delivery Reviews*, Biomimetic approaches in bone tissue engineering: Integrating biological and physicomechanical strategies, 84: 1-29, Fernandez-Yague *et al*, 2015, with permission from Elsevier)

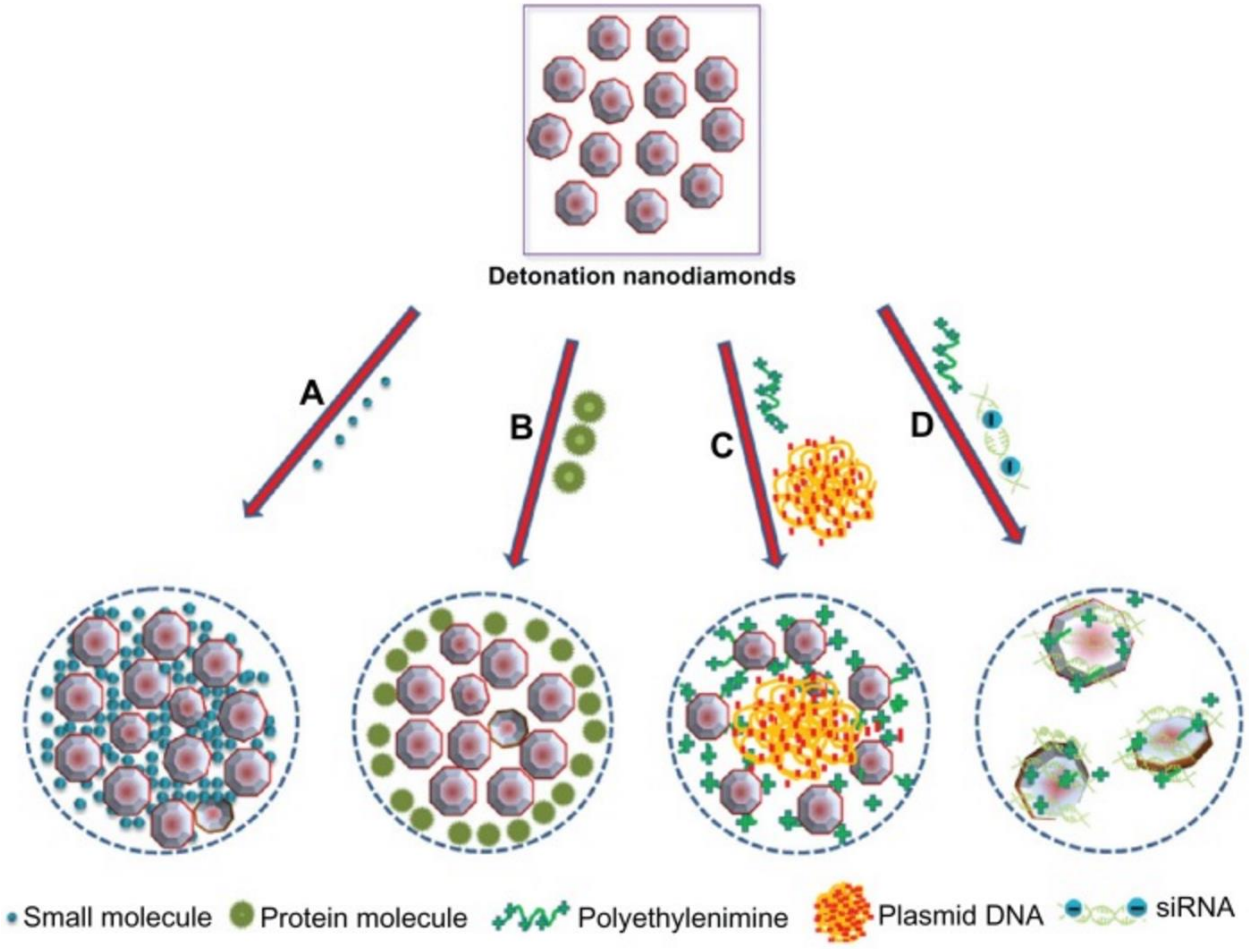

Figure 1.2

Nanodiamond-based Drug Delivery. Nanodiamonds, with some modification, are capable of delivering a wide variety of therapeutic types. Small molecules and proteins adsorb to the surface of carboxylated NDs in many cases, while delivery of nucleic acids can be achieved by first complexing NDs with positively charged polymers, such as polyethylenimine. (Reproduced from Kaur *et al*, International Journal of Nanomedicine, 2013, with permission from DovePress)

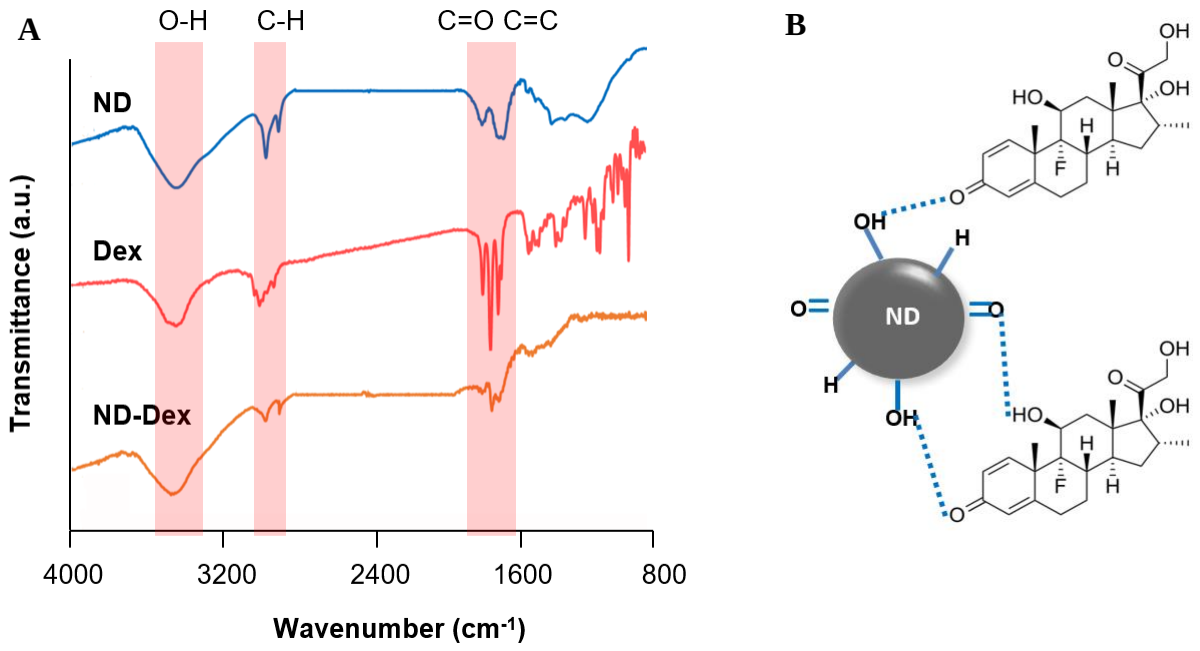

Figure 2.1

FTIR Spectra of ND-Dex and Proposed Interactions. (A) Characteristic peaks of both NDs and Dex are visible in the complex. (B) Schematic representing the possible interactions between Dex and the surface of NDs. Hydrogen bonds are highlighted in blue.

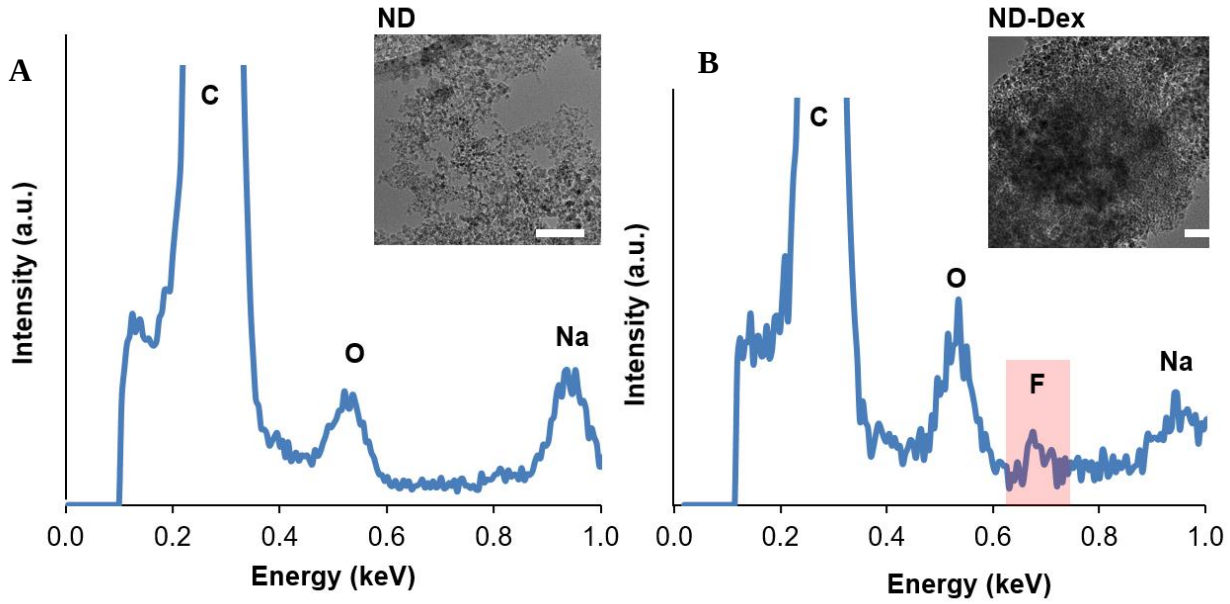

Figure 2.2

TEM/EDX Analysis. (A) TEM/EDX analysis of ND suspension. TEM images showing well-dispersed NDs suspension in water (Scale bar = 20 nm). EDX analysis showed the presence of carbon and oxygen on the NDs surface. (B) TEM/EDX analysis of ND-Dex complex revealed the presence of fluorine, confirming the adsorption of Dex onto the NDs surface.

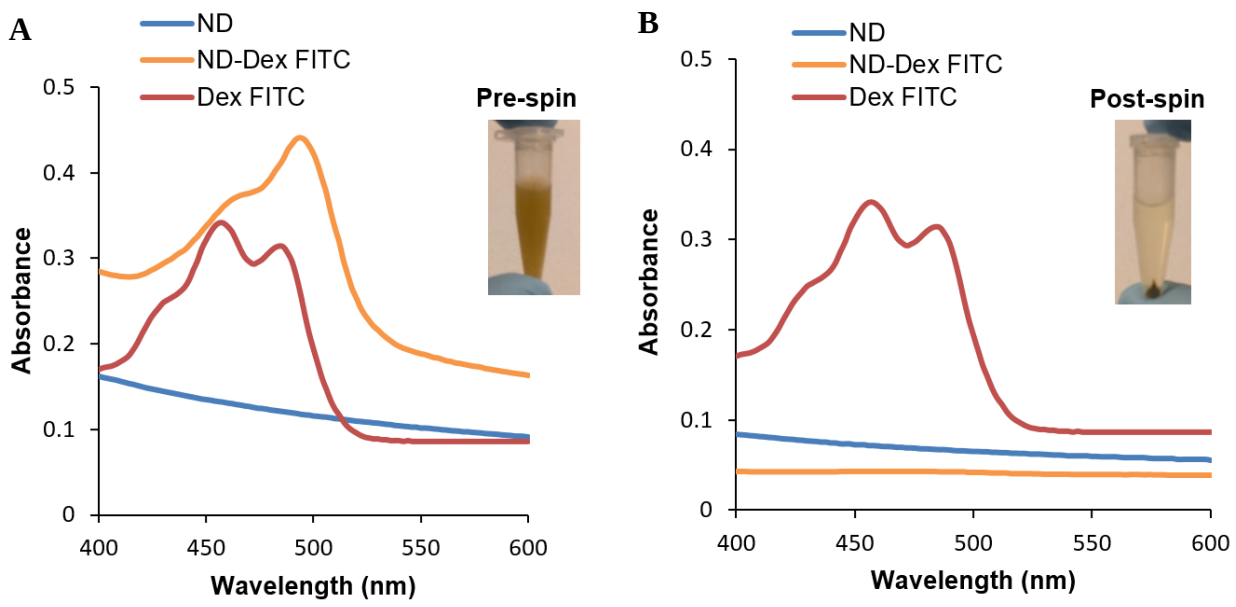

Figure 2.3

UV-Visible spectra of NDs and ND-Dex-FITC complex pre- and post- centrifugation (A) Picture showing the suspension of NDs and Dex-FITC prior to centrifugation. Complex was formed by mixing Dex-FITC and NDs at a ratio of 1:10. UV-Vis spectra of the ND suspension, Dex-FITC and the complex in the range of 400-600 nm. (B) UV-Vis spectra showing the disappearance of the peak relative to the ND-Dex FITC complex compared to the solution of Dex-FITC which showed the same absorbance before and after centrifugation.

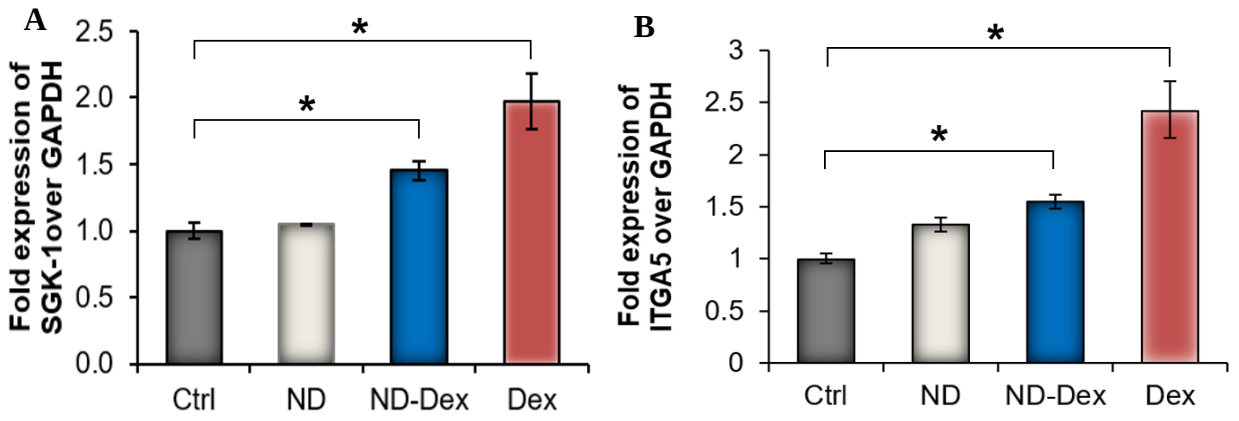

Figure 2.4

qPCR analysis of Dex-induced genes in hASCs. (A) Relative expression of SGK-1, following one hour of exposure to hASCs. Both Dex and the ND-Dex complex respectively showed a significant increase in SGK-1 expression. (B) Relative expression of cytoskeletal element integrin α5 (ITGA5) following six hours of exposure to hASCs. ND-Dex and Dex both significantly increased the expression of integrin α5 (* = $p < 0.05$, $n = 3$).

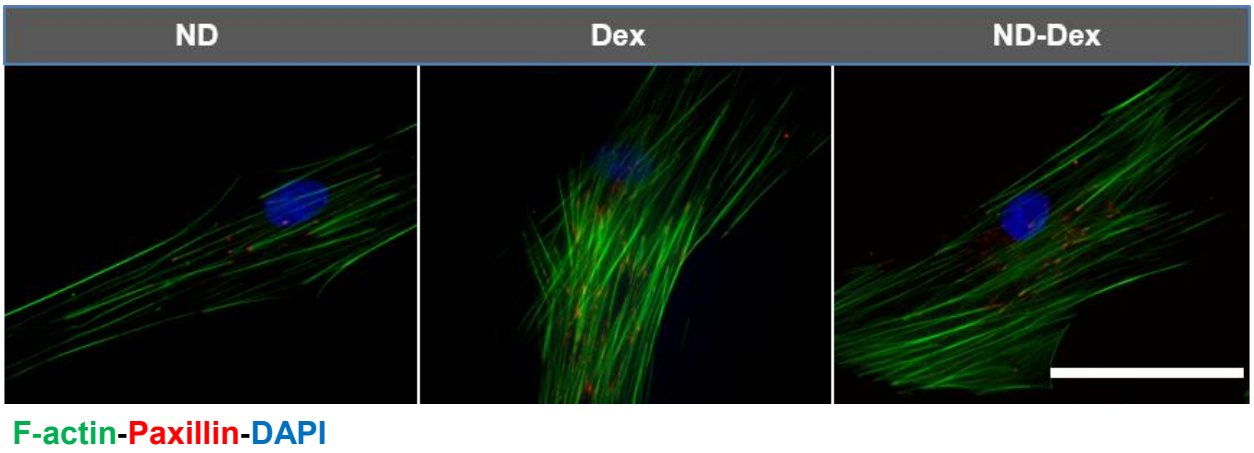

Figure 2.5

Focal Adhesion Staining After Dex Exposure. Fluorescence immunostaining of paxillin for hASCs showing an increase in the number of focal adhesion after 24 hours of Dex exposure. The ND/Dex complex was able to induce similar paxillin expression as the drug alone. (Scale bar = 20 μm).

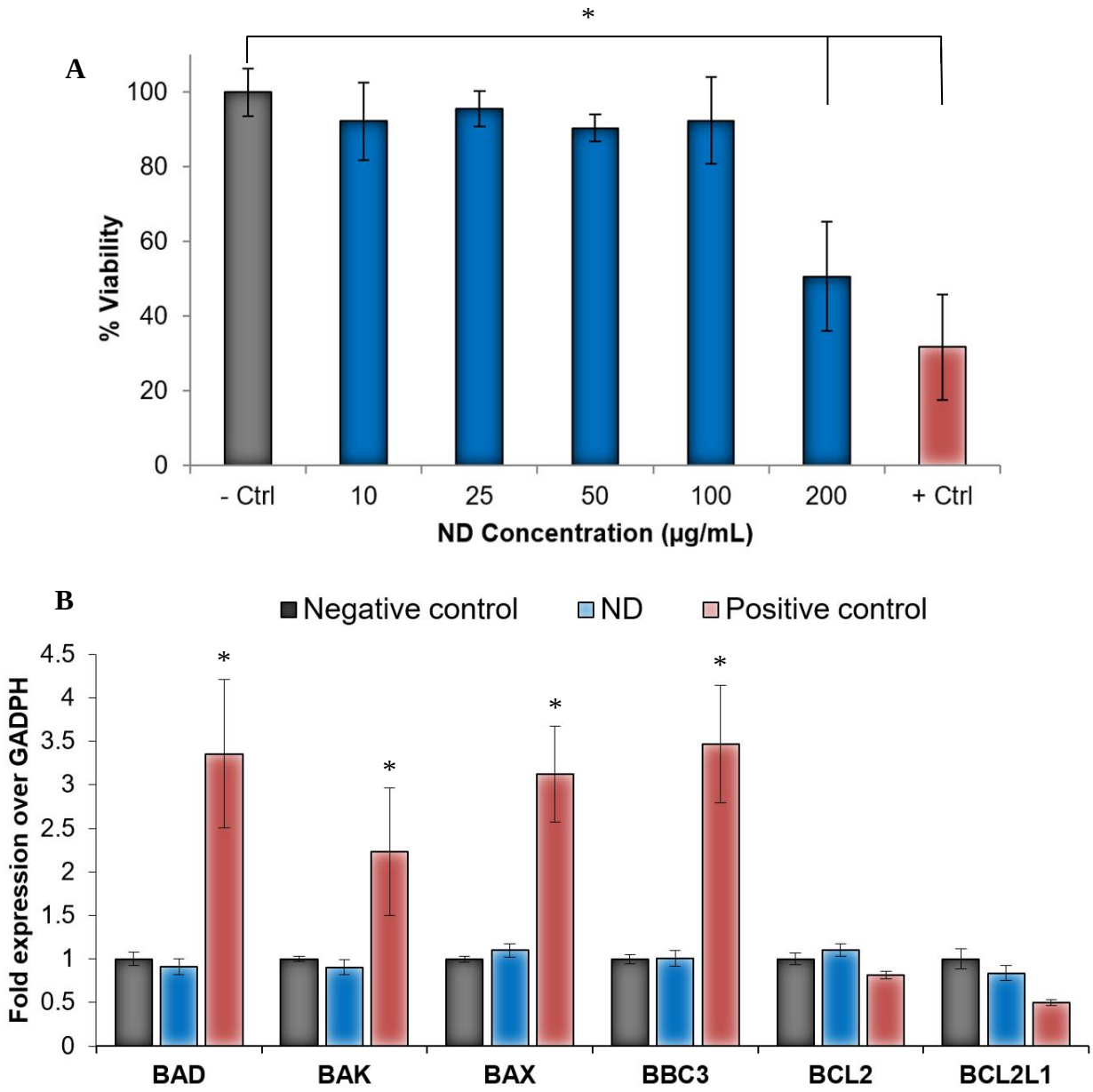

Figure 2.6

Biocompatibility Analysis of NDs in 2D. (A) MTT Assay of hASCs exposed to varying concentrations of NDs. Up until 200 µg/mL, NDs showed no significant toxicity. (B) qPCR analysis of a variety of apoptotic markers. hASCs exposed to 25 µg/mL showed no significant change in expression of a variety of pro-apoptotic and anti-apoptotic markers. (* = $p < 0.05$, n=3).

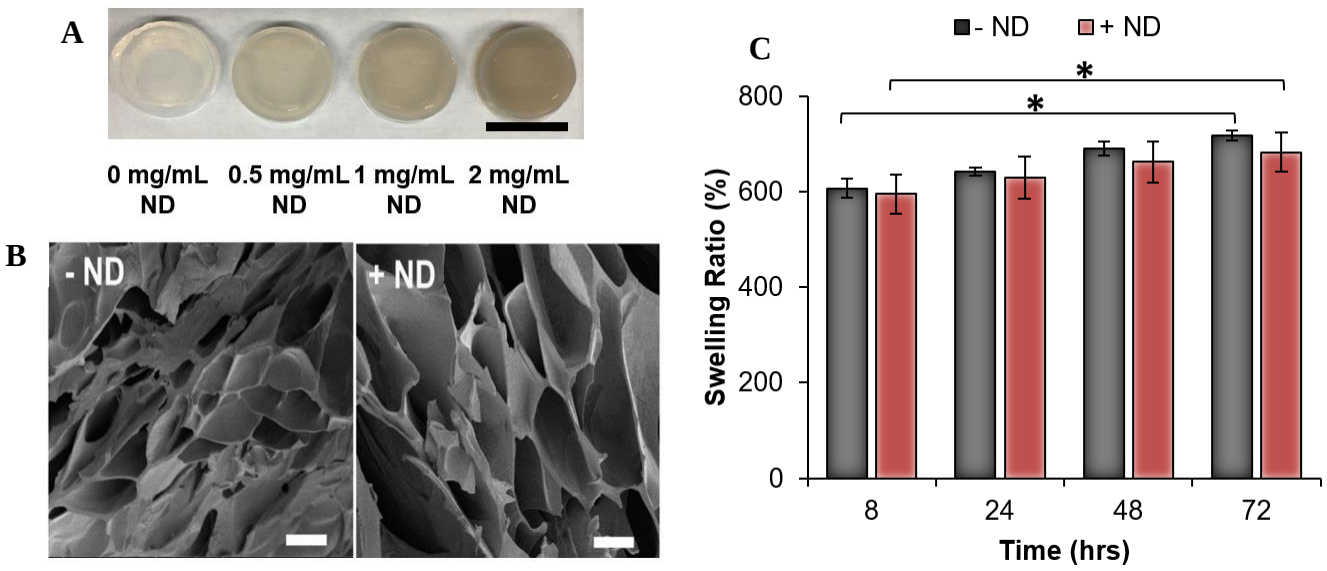

Figure 2.7

Nanocomposite hydrogel physical characterization. (A) Images of nanocomposite hydrogels with increasing concentration of NDs. (Scale bar = 15 mm). (B) SEM images of GelMA scaffold with and without NDs showing similar porosity. (Scale bar = 100 µm). (C) Swelling ratio of nanocomposite hydrogels over time showing a steady increase in the values for both groups (* = $p < 0.05$, n=5).

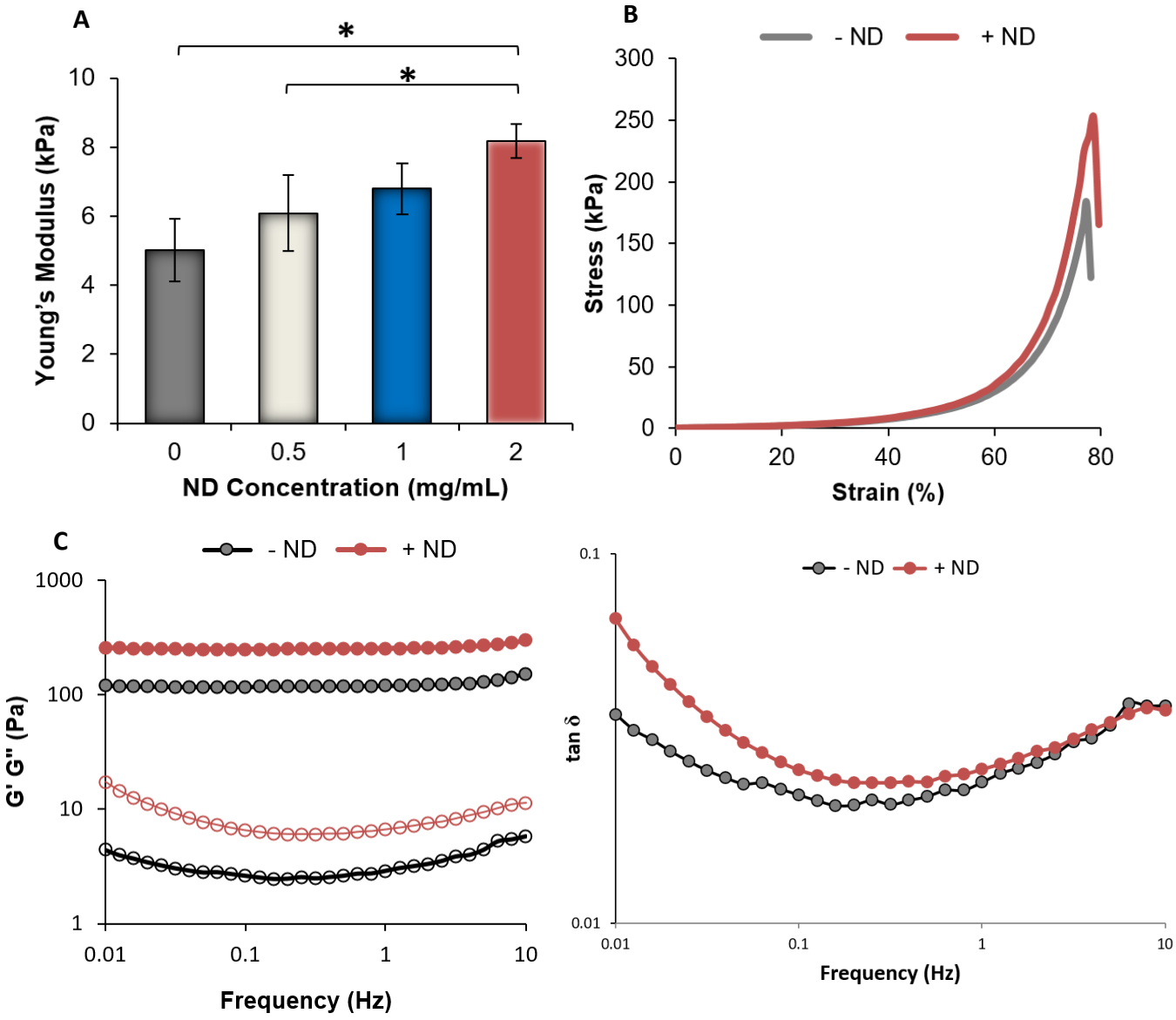

Figure 2.8

Mechanical and rheological studies of ND-GelMA nanocomposites hydrogels. (A) Young's modulus of different nanocomposite hydrogels with varying concentration of NDs. A significant increase was observed for the group containing 2 mg/mL of NDs. (* = $p < 0.05$, n=4). (B) Stress strain curves obtained after uniaxial compression showing an increase in the ultimate fracture strength for the group containing NDs at the concentration of 2 mg/mL. (C) Frequency sweeps carried out in the range of 0.01 up to 10 Hz showed an increase in the value of the storage modulus (G') for the system containing NDs. The increase could be attributed to noncovalent interactions between the NDs and the polymeric matrix. (D) Tan delta plots of the frequency sweeps

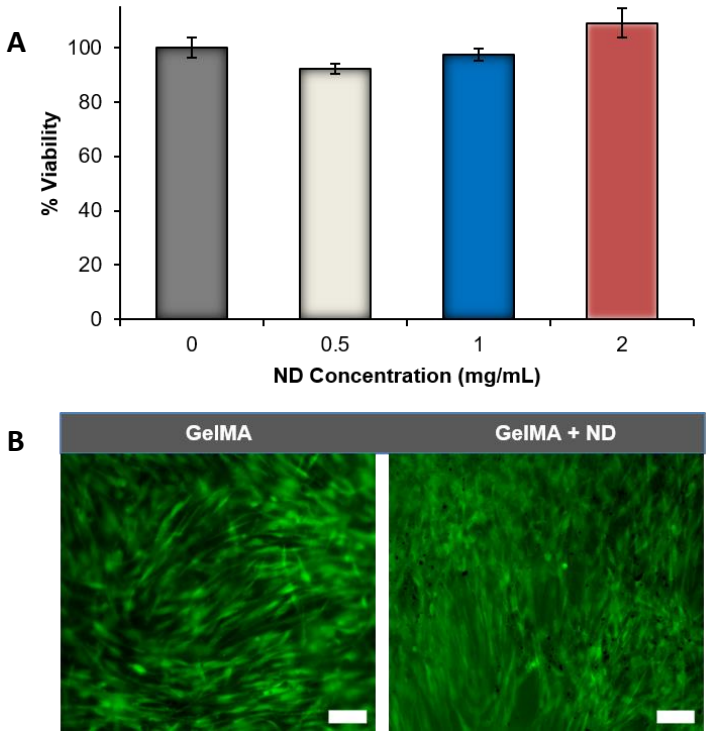

Figure 2.9

Nanocomposite Biocompatibility and 3D hASC Encapsulation. (A) MTT study of hASCs encapsulated in the nanocomposite GelMA hydrogels showed excellent biocompatibility regardless of the ND concentration (0-2 mg/mL). (B) Calcein-AM staining indicated hASCs spindle-like morphology and stretching throughout the network for both groups (ND concentration = 2 mg/mL) (Scale bar = 100 μm).

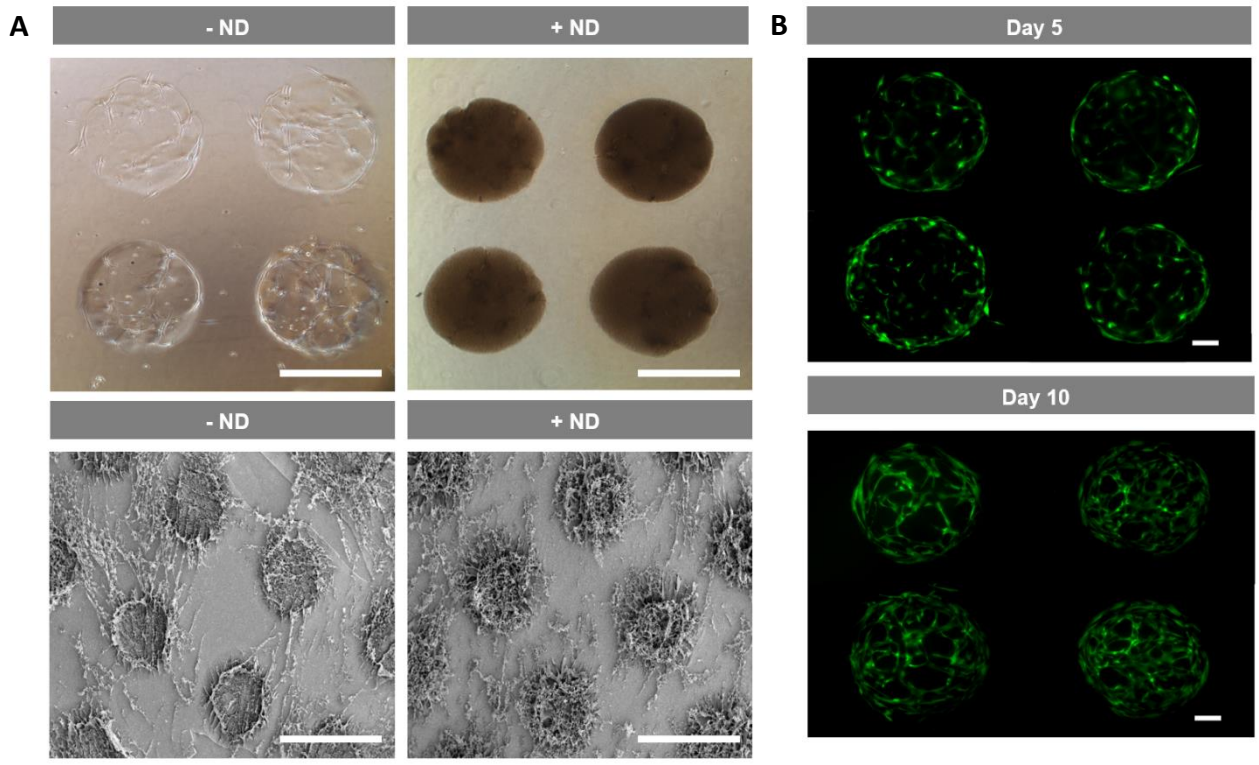

Figure 2.10

Nanocomposite Micropatterning and 3D hASC Encapsulation (A) Brightfield images (top) and SEM images (bottom) of 1 mm cylindrical GelMA and GelMA-ND micropatterns. (Brightfield scale bar = 1 mm, SEM scale bar = 500 μm) (B) Calcein-AM staining of hASCs at 5 and 10 days showed that cells were viable within the micropatterned nanocomposites. (Scale bar = 200 μm)

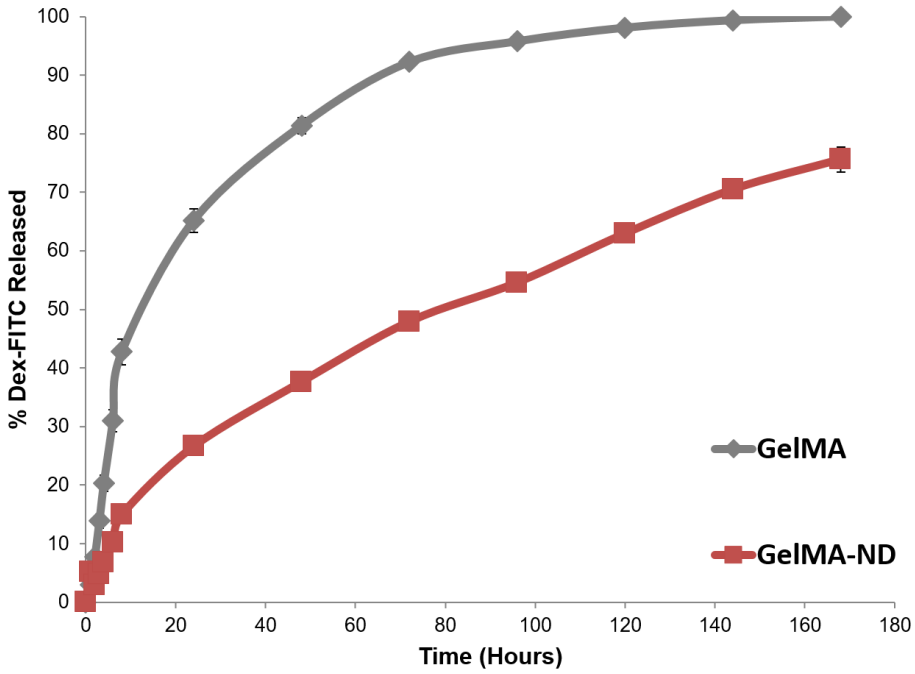

Figure 2.11

Dex-FITC Release from Nanocomposites. Nanocomposite hydrogels significantly extended the release of Dex-FITC. At three days, only half of Dex-FITC had eluted out of the nanocomposites, compared to >90% release from hydrogels lacking NDs.

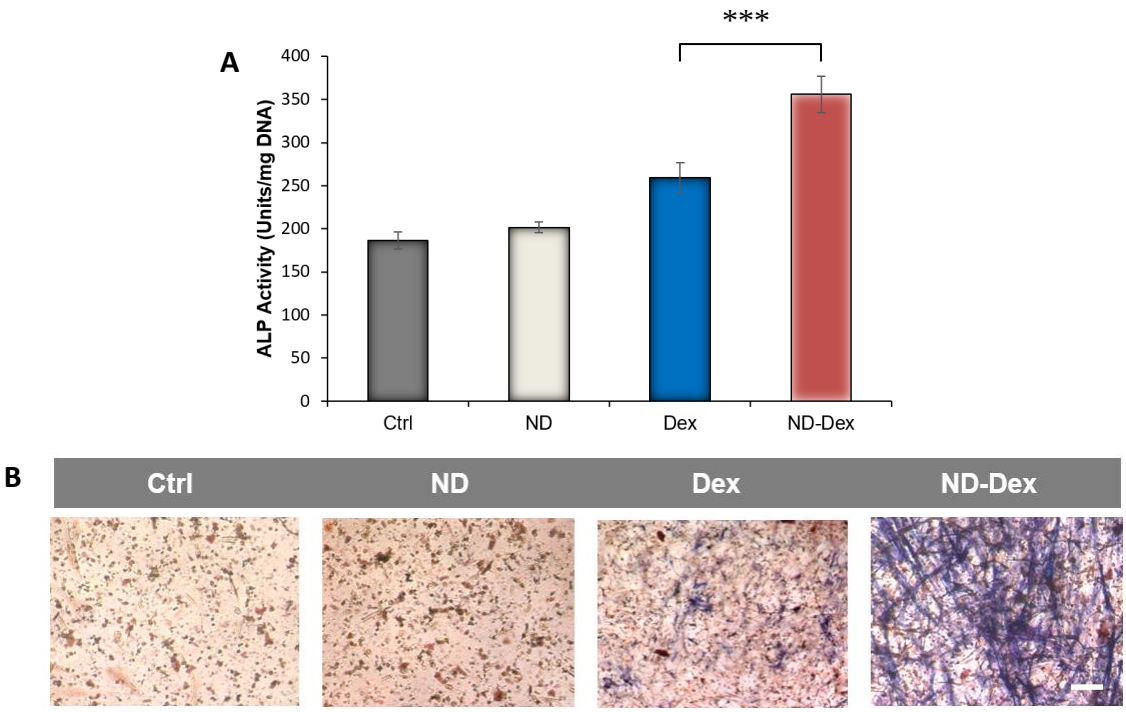

Figure 2.12

ALP Differentiation Studies. (A) ALP quantification of hASCs after 14 days of culture in osteoconductive media showing a significant increase in ALP expression for the nanocomposite system compared to control groups. (*** = $p < 0.001$, n=3). (B) ALP staining of hASCs encapsulated in GelMA hydrogels indicating a higher expression of ALP in the group containing the complex ND-Dex after 14 days. (Scale bar = 100 µm).

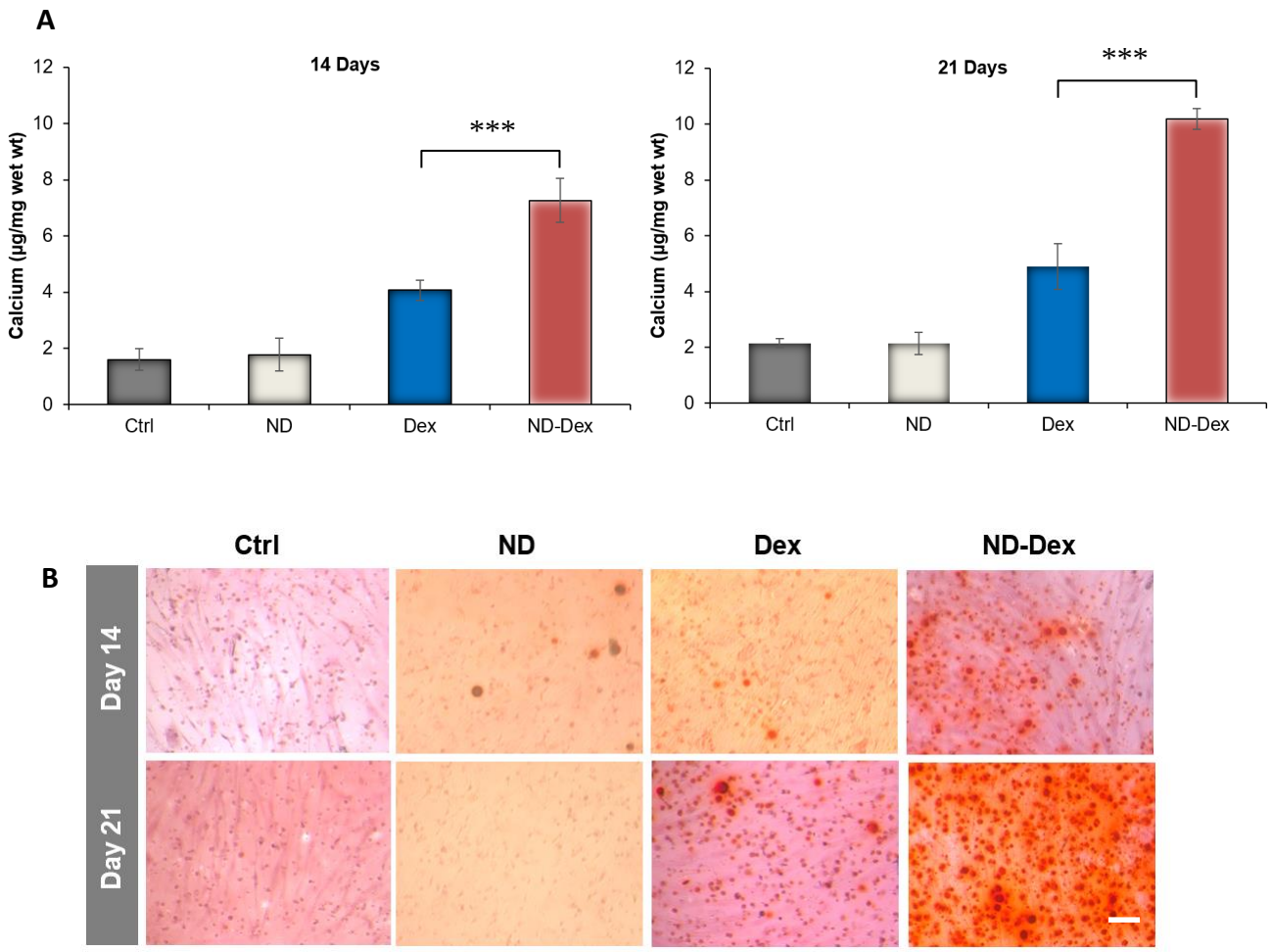

Figure 2.13

Alizarin Red Staining and Quantification. (A) Calcium quantification after 14 and 21 days of hASC differentiation using osteoconductive media. At both times points a higher amount of calcium was detected for the ND-Dex group compared to the other groups tested (*** = $p < 0.001$ n =3). (B) Calcium was quantified by colorimetric assay and observed using Alizarin Red S staining at 14 days and 21 days. This staining qualitatively confirmed the higher amount of calcium in the ND/Dex group. (Scale bar = 100 µm).

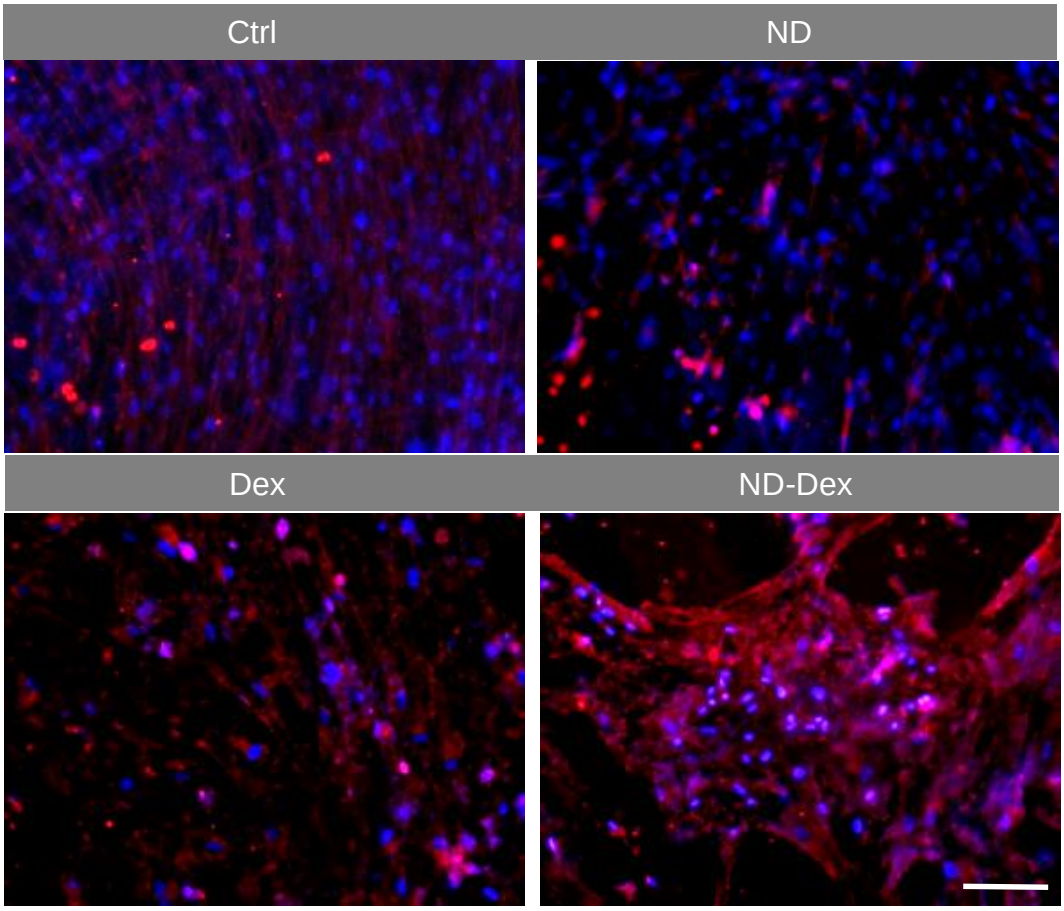

Figure 2.14

Osteocalcin Staining. Encapsulated hASCs were stained for osteocalcin, a gene associated with hydroxyapatite binding and solely secreted by osteoblasts, after 21 days. Significantly more staining in the ND-Dex group was observed compared to controls. (Scale bar = 100 μm)

Contributions to Knowledge

I. Publications:

R Maloney, S Pacelli, A Chakravarti, R Waters, A Paul*. Gelatin-nanodiamond composite for drug delivery and bone tissue engineering. (To be submitted)

R Waters, S Pacelli, **R Maloney**, I Medhi, R PH Ahmed, A Paul* (2016) Stem cell secretome-rich hydrogel: a dual action cardiovascular therapy. *Nanoscale* 8(14):7371-6.

II. Book Chapters:

R Maloney, A Mondal, I Medhi, R Ahmed, A Paul* (2016). Functional Nucleic Acid Incorporated Materials for Cell Therapy and Tissue Engineering. Book: Fundamental Principles of Smart Materials for Tissue Engineering. Publisher: Royal Society of Chemistry. Editor: Qun Wang.

R Waters, **R Maloney**, SH Ranganath, H Hsieh, A Paul* (2016). Nano- and Micro-Scale Delivery Systems for Cardiovascular Therapy. Pages 269-89. Book: Microscale Technologies for Cellular Engineering. Publisher: Springer. Editor: A Singh and A Gaharwar.

III. Conference Presentations:

R Waters, S Pacelli, **R Maloney**, I Medhi, R PH Ahmed, A Paul* (2015) Local delivery of stem cell growth factors with injectable hydrogels for myocardial therapy. World Biomaterials Congress, May 2016. (Oral Presentation)

R Maloney, S Pacelli, A Chakravarti, R Waters, A Paul*. Gelatin-nanodiamond composite for drug delivery and bone tissue engineering. World Biomaterials Congress, May 2016. (Poster Presentation)

R Maloney, S Pacelli, A Chakravarti, R Waters, A Paul*. Gelatin-nanodiamond composite for drug delivery and bone tissue engineering. KU Graduate Engineering Association Research Competition, April 2016. (Oral Presentation)

R Waters, S Pacelli, **R Maloney**, I Medhi, R PH Ahmed, A Paul* (2015) Local delivery of stem cell growth factors with injectable hydrogels for myocardial therapy. KU Graduate Engineering Association Research Competition, April 2016. (Poster Presentation)

R Waters, S Pacelli, **R Maloney**, I Medhi, R PH Ahmed, A Paul* (2015) Local delivery of stem cell growth factors with injectable hydrogels for myocardial therapy. KU Graduate Research Competition, March 2016. (Poster Presentation)

R Waters, S Pacelli, **R Maloney**, I Medhi, R PH Ahmed, A Paul* (2015) Local delivery of stem cell growth factors with injectable hydrogels for myocardial therapy. Capitol Graduate Research Summit, February 2016. (Poster Presentation)